NANO · MICRO small
www.small-journal.com

Valleytronics: Fundamental Challenges and Materials Beyond Transition Metal Chalcogenides

Rui Xu, Zhiguo Zhang, Jia Liang, and Hanyu Zhu**

Valleytronics, harnessing the valley degree of freedom in the momentum space, is a potential energy-efficient approach for information encoding, manipulation, and storage. Valley degree of freedom exists in a few conventional semiconductors, but recently the emerging 2D materials, such as monolayer transition-metal dichalcogenides (TMDs), are considered more ideal for valleytronics, due to the additional protection from spin-valley locking enabled by their inversion symmetry breaking and large spin-orbit coupling. However, current limitations in the valley lifetime, operation temperature, and light-valley conversion efficiency in existing materials encumber the practical applications of valleytronics. In this article, the valley depolarization mechanisms and recent progress of novel materials are systematically reviewed for valleytronics beyond TMDs. Valley physics is first reviewed and the factors determining the valley lifetime, including the intrinsic electron-electron and electron-lattice interactions, as well as extrinsic defect effects. Then, experimentally demonstrated and theoretically proposed valley materials are introduced which potentially improve valley properties through the changes of spin-orbit coupling, electronic interactions, time-reversal symmetry, structures, and defects. Finally, the challenges and perspectives are summarized to realize valleytronic devices in the future.

1. Introduction

Certain crystalline semiconductors have degenerated but nonequivalent band edge states at different locations in the momentum space. In such materials, the carriers possess a valley degree of freedom in addition to charge and spin degrees of freedom.[1] Manipulating the valley degree of freedom for information encoding, processing, and storage enables a new electronic property, termed "valleytronics", which potentially offers many advantages such as low energy consumption,[2] fast processing speed,[3] non-volatility,[4,5] and long transmission[6] over conventional charge-based electronics. The inherent physical properties are crucial for useful valleytronics: The ideal materials for the applications of valleytronics should feature a band structure with two (or more) electronic pockets that are same in energy but as different as possible in wavefunctions to prevent intervalley scattering. As the information is stored in the momentum space, the periodicity and quality of the materials is also very important.

While conventional semiconductors like diamond,[7] silicon,[8–10] aluminum arsenide,[11] and bismuth[12] contain inequivalent valleys, it is difficult to achieve the selective initialization, manipulation, and readout the valley states due to the weak coupling between the valley index and external fields in these materials. After the discovery of graphene in 2004, valleytronics has entered a period of rapid growth.[13,14] In the hexagonal honeycomb structure of graphene, two valleys are present at the +K and -K points at the vortices of the hexagonal Brillouin zone. Unfortunately, carriers in the two valleys of graphene can be thermally excited due to graphene's zero bandgap, so the valley polarization is not stable at room temperature. Intriguingly, 2D transition-metal dichalcogenides (TMDs) opened new opportunities to manipulate the valley degree of freedom because they share a honeycomb structure with graphene but possess a non-zero direct bandgap.[1] Moreover, the inversion symmetry of monolayer TMDs is spontaneously broken, leading to opposite values of Berry curvature, orbital magnetic moments, and optical selection rule at ±K points.[15] Under the excitation of circularly polarized light, monolayer TMDs can convert the light polarization information into electronic information.[16–18] In addition, external electric and magnetic fields can also manipulate the valley index in monolayer TMDs by coupling to the valley contrasted anomalous transport and magnetic moments, respectively.[3,19] Therefore, monolayer TMDs and their derivatives are considered outstanding platforms for exploring valleytronics. Over the years, there has been remarkable advances in valleytronics based on TMDs, as summarized by quite a few excellent reviews.[3,20–24] However, valleytronics still encounters many challenges, including short valley lifetime,[25,26] stringent requirements for monolayers,[18] and low operating temperature.[16] Therefore, it is essential to

R. Xu, H. Zhu
Department of Materials Science and NanoEngineering
Rice University
Houston, Texas 77005, USA
E-mail: hz67@rice.edu
Z. Zhang, J. Liang
Department of Materials Science
Fudan University
Shanghai 200433, China
E-mail: jialiang@fudan.edu.cn
The ORCID identification number(s) for the author(s) of this article can be found under https://doi.org/10.1002/smll.202402139

DOI: 10.1002/smll.202402139

explore alternative valleytronics materials beyond TMDs, which may pave the way for future exploration of room temperature valleytronic devices.

In this review, we systematically review the recent progress in novel materials for valleytronics beyond TMDs. First, we discuss the physical processes that limit the valley lifetime, which is a critical consideration for information processing. Although there are very limited studies on valley dynamics outside TMDs and graphene, the fundamental physics discovered in conventional valleytronic systems are likely generalizable to new materials. The intrinsic mechanisms for scattering the valley excitons and free carriers are different, and defects (point defects and line defects) play an important role in the process too. Based on these discussions, we then summarize the recently proposed non-TMD valleytronic materials from experimental observations and theoretical predictions. We cover both new materials in hexagonal and non-hexagonal structures, as well as graphene and heterostructures between TMD and non-TMD materials in which new valleytronic properties are enabled by many-body effects and band-structure engineering, respectively. A few experiments showed promise for robust valley polarization at elevated temperatures but lacked detailed dynamics or transport measurements yet to directly compare with TMDs. Most of the works are theoretical predictions for new valley manipulation methods, new phases of matter, or large valley splitting that still await experimental validations. Finally, we outline the remaining challenges facing the valleytronic field and possible opportunities to realize practical valleytronic devices.

2. Intrinsic and Extrinsic Valley Lifetime

To develop new valleytronic materials, we first conduct an overview of the key performance parameters and bottlenecks of existing materials. First and foremost, a long valley lifetime is crucial for storing and processing valley information. For any valley polarization carriers, including excitons, electronic free carriers, or bosonic excitations in materials, the valley lifetime is governed by both the lifetime of the excitation themselves, indicating how long a non-equilibrium particle distribution can exist before thermalization, and the valley depolarization lifetime, indicating how long the particles take to scatter into the opposite valley. Generally, the scattering rate can be reduced by the presence of an energy gap, either from band structure or opened by electronic interactions. For example, monolayer graphene has very elegant valley physics, but the carriers are located at a gapless Dirac cone with scattering lifetime at picosecond time scale.[27] By contrast, in monolayer TMDs, because of the large bandgap over 1 eV, the valley information can be injected in the form of polarized excitons, whose lifetime can be longer than nanoseconds with careful sample preparations under cryogenic temperature.[28,29] Thus, the valley lifetime is in turn limited by intervalley scattering from exciton exchange interactions, which is measured to be around picosecond scale. The exchange scattering can be suppressed by separating the electrons and holes, extending valley scattering lifetime by orders of magnitude up to microseconds as observed in experiments,[30,31] leading to long valley diffusion length on the order of 10 μm.[6] Ultimately, using many-body effects and external magnetic fields to lift the valley degeneracy, the valley lifetime in gapped bilayer graphene quantum dots approaches 500 ms.[32] While impressive, these results are only obtained in very low temperatures to reduce the ubiquitous electron-phonon coupling, and hence cannot directly be applied to ambient solid-state devices. Besides, charged valley carriers are sensitive to the electromagnetic environment, so their quantum coherence lifetime (T_2) is generally much shorter than their population lifetime (T_1). Therefore, to harness quantum valleytronics, charge-neutral bosonic excitations such as phonons may have advantage, whose lifetime may reach nanoseconds even at room temperature in the cases of certain out-of-plane acoustic modes because the anharmonic scattering is suppressed for the lowest phonon branch.[33,34] As of now, there is no experimental proof of either population or coherence lifetime of valley phonons, so we will focus on electronic valley carriers in this review. Overall, fundamental valley physics has been well-established and already demonstrated excellent performance with existing materials like graphene and TMDs under extreme conditions. Although new physics may still emerge in the future, we expect the same principles summarized in this section should apply to most new valleytronic materials, whose main purpose is to function under more robust conditions for potential applications.

2.1. The Valley Lifetime of Excitons

The valley depolarization lifetime of neutral exciton is primarily determined by the electron-hole exchange interaction, known as Maialle–Silva–Sham (MSS) mechanism.[35] This mechanism involves an interband process between conduction and valence states, leading to virtual annihilation of an exciton in one valley and its creation in the opposite valley (**Figure 1a**).

Since bright excitons always possess a total momentum and spin of zero, they do not require any change in momentum or spin to scatter to the other valleys, making the exchange interaction to be more effective. This interaction couples the two bright excitons in opposite valleys and thus behaves like an in-plane effective magnetic field with respect to the valley pseudospin. The magnitude of this effective magnetic field depends on the magnitude of the exciton momentum k. The direction of the effective magnetic field is determined by the direction of k; the field rotates 360° when k rotates 180°. The k-dependent exchange interaction, combined with momentum scattering by phonons, results in a finite and varying in-plane effective magnetic field, which leads to exciton valley depolarization.[3] In the following discussion, we take TMDs as an example, but note that such mechanism is general for any two-valley direct-gap semiconductors.[36,37]

The exciton binding energy in 2D TMDs is within the range of 0.6–1 eV,[38,39] indicating a significant mixture of electron and hole wavefunctions and, consequently, a strong electron-hole exchange interaction. This would lead to a strong suppression in terms of exciton valley lifetime. Previous theoretical works have shown that the exchange interaction can be divided into the long-range (L-R) and short-range (S-R) parts.[40] Both parts can cause inter- and intravalley bright exciton transitions. However, the intravalley bright exciton transition channel is nearly forbidden due to the large splitting of the valence bands, and only the intervalley exchange interaction can efficiently cause the valley depolarization. For the A exciton, which is the first optical excitation in TMD monolayers formed

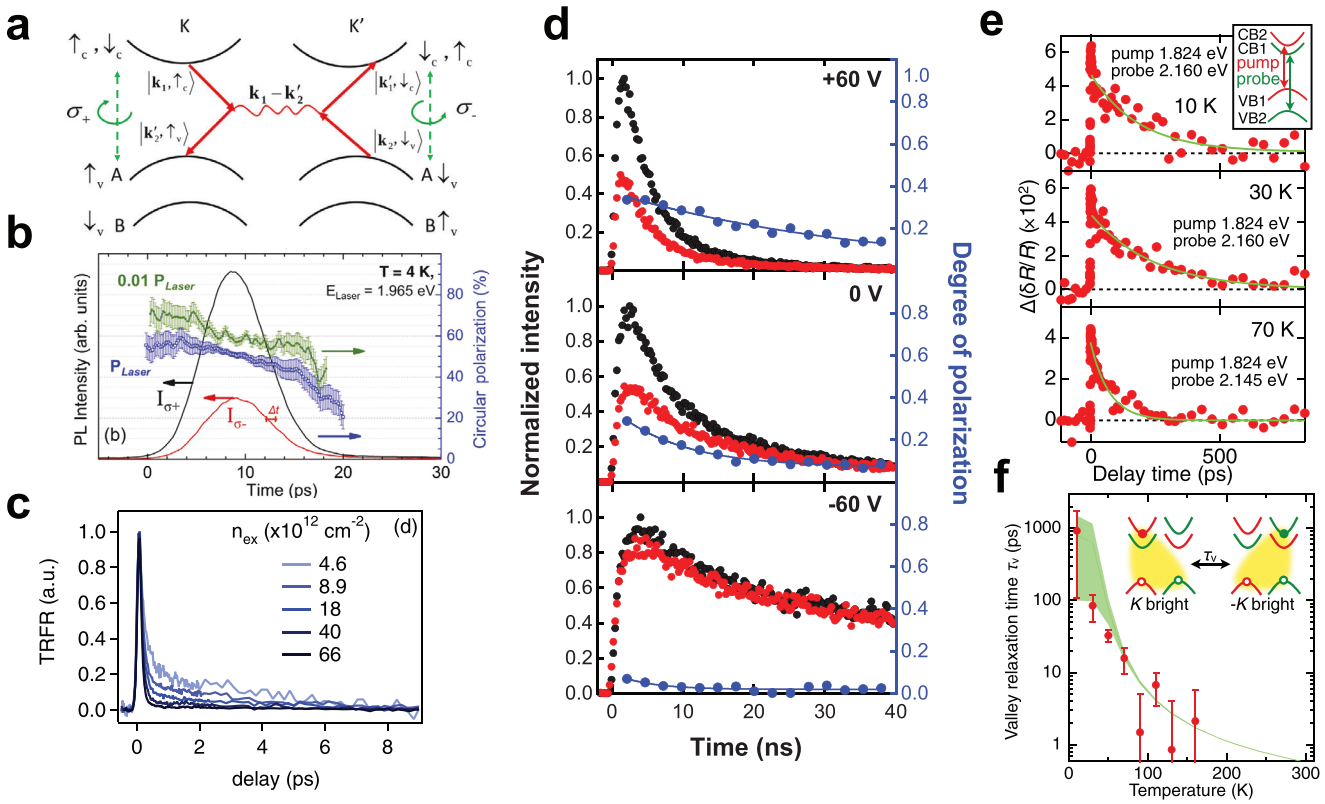

Figure 1. a) Feynman diagram of intervalley scattering of neutral exciton via Maialle–Silva–Sham (MSS) mechanism in monolayer TMDs. Due to the short-range exchange interaction, the electrons at conduction (valence) band at K (K') valley with momentums of $\mathbf{k}_1$ ($\mathbf{k}_2$) are scattered to the K'(K) valley, respectively. Consequently, the intervalley bright exciton scattering is mediated by the virtual recombination of a bright exciton in the K valley and then generation in the K' valley, or vice versa. Reproduced with permission.[40] Copyright 2014, American Physical Society. b) Left axis: Time-resolved co- and cross-polarized PL emission intensity from neutral excitons in monolayer MoS_2 at 4 K under left circularly polarized ($\sigma+$) excitation. Right axis: Valley polarization as a function of time, indicating a depolarization lifetime of ≈20 ps. Reproduced with permission.[25] Copyright 2014, American Physical Society. c) Normalized time-resolved Faraday rotation measurement under circular polarized pumping on monolayer MoS_2 as a function of exciton density. Reproduced with permission.[47] Copyright 2015, American Physical Society. d) Time-resolved interlayer exciton PL at selected gate voltages. Co- and cross- polarized PL are shown in black and red dots, respectively. The blue curve (right axis) shows the decay of valley polarization. Interlayer excitons lifetime reaches up to 39 ± 2 ns for gate voltages of +60V and reduces at other gating conditions. Reproduced with permission.[54] Copyright 2016, American Association for the Advancement of Science (AAAS). e) Pump-probe transient reflection measurement near the B transition (inset) of positive trions in monolayer WSe_2 at varying temperatures. Reproduced with permission.[56] Copyright 2019, American Physical Society. f) Temperature dependent valley relaxation lifetime of positive trions. The lifetime at 4 K can be over 100 ps. Reproduced with permission.[56] Copyright 2019, American Physical Society.

by the electron-hole pair at the conduction and valence band edge with a small center-of-mass momentum,[41] the intervalley exciton transition is relatively slow, which leads to the existence of residual valley polarization predicted to last on the picosecond scale. So far, numerous works have attempted to measure exciton valley lifetimes in monolayer TMD materials using various techniques, including time-resolved photoluminescence (PL)[25,42] (Figure 1b), transient absorption or reflection,[26,43,44] time-resolved magneto-optics spectroscopy,[30,45–47] and nonlinear optical spectroscopies.[48] These studies consistently show a valley lifetime of picosecond scale for neutral bright excitons in mechanical exfoliated samples under cryogenic temperature, agreeing with the theoretical results. Additionally, photoexcitation power-dependent magneto-optical measurements revealed that faster exciton valley depolarization at higher exciton densities (Figure 1c), indicating that the intervalley scattering rate of neutral excitons increases by an order of magnitude at higher photoexcited exciton densities. It implies that the valley relaxation processes in TMDs occurs in a weak scattering regime, where momentum decay time and valley lifetime are proportional, paving the way to other possible extrinsic relaxation channels, like Elliot-Yafet (EY) mechanism, involving the scattering with defects and phonons, which would play some roles in the slow valley decay component.[47,49]

In order to reduce the effect of MSS mechanism and increase the exciton valley lifetime, researchers have been exploring methods to ease or even get rid of the exchange interaction. One effective method is to fabricate type-II van der Waals (vdW) heterostructure, where electrons and holes are separated into different layers in both real space and momentum space because of the band alignment,[50] giving rise to interlayer excitons.[22,50–53] Since the strength of the electron–hole exchange interaction is directly proportional to the electron–hole overlap probability, the spatial separation of electrons and holes greatly reduces the

impact of electron–hole exchange interaction, leading to a much longer valley lifetime. The charge transfer process in semiconducting heterostructures occurs very rapidly, typically on femtosecond scale,[50] long before the exchange interaction becomes prominent. Indeed, an improved valley lifetime up to 40 ns for interlayer excitons has been observed in $MoSe_2$-WSe_2 heterostructure under electrostatic gating[54] (Figure 1d). Meanwhile, converting neutral excitons into other information carriers with non-zero total momentum and/or spin serves as another avenue to improve the valley lifetime. For example, a valley lifetime exceeding 100 ps at cryogenic temperature has been observed in charged excitons, or trions, in monolayer WSe_2[30,55,56] (Figure 1e,f), which suggests that the electron-hole exchange interaction is reduced in three-body trion systems due to the presence of additional carriers. Similar results are also observed in biexcitons, indicating nontrivial many-body interactions among the charged particles.[57,58]

2.2. The Valley Lifetime of Free Carriers

Without exchange interaction, the valley polarization of a single charged carrier is expected to be prolonged. However, in most valleytronics materials studied at the early stage of the field, such as silicon, the scattering between degenerate valleys still keeps valley lifetime short.[59,60] To lift the valley degeneracy, one can either apply external strain or magnetic fields,[61,62] or find new materials with strong spin-orbit coupling (SOC) such as TMDs. Due to SOC and inversion symmetry breaking in monolayer TMD crystals, the spin of electrons/holes is opposite at the band edge of the two valleys, which is known as the spin-valley locking effect.[15,63,64] This implies that valley depolarization of carriers shall be accompanied by a simultaneous momentum change and a flip of spin. Thus, for free carriers with non-zero total momentum and spin, the spin relaxation lifetime becomes crucial in valley depolarization. The spin lifetime of carriers τ_s in monolayer TMDs is typically on the order of nanoseconds for electrons[30,31,65] and up to microsecond scale for holes,[6,31,66] which are superior candidates for valleytronic applications compared to excitons. More generally, any new materials with strong magnetism, large SOC, or placed under proper magnetic fields can potentially suppress valley scattering and exhibit a longer carrier valley lifetime.

Four mechanisms are usually discussed for spin relaxation in semiconductors, including the D'yakonov-Perel', Elliot-Yafet, Bir-Aronov-Pikus, and hyperfine-interaction mechanisms. Among them, the hyperfine-interaction mechanism, accounting for the interaction between carrier spins and nuclei, can be neglected as long as the orbital wavefunctions have small overlap with the nucleus (i.e., other than s orbitals).[18,67] The D'yakonov-Perel' and Elliot-Yafet mechanisms are mediated by the SOC of crystals. The Bir-Aronov-Pikus (BAP) mechanism accounts for electron spin-flip processes mediated by the electron-hole exchange interaction, and it is usually only relevant in heavily p-doped semiconductors.[68] Here, we will discuss D'yakonov-Perel', Elliot-Yafet mechanisms, and Bir-Aronov-Pikus mechanisms further in the following sections.

2.2.1. D'yakonov-Perel' (DP) Mechanism

The D'yakonov-Perel' (DP) mechanism accounts for spin precession between scattering events induced by the SOC when the inversion symmetry of the crystal is broken.[67] The lack of inversion symmetry will lift the degeneracy of the spin-up and down states of the carriers in the energy band, making SOC to be an effective k-dependent magnetic field.[69] Any momentum scattering event causes the electron (hole) to experience different effective fields and precession rate would, consequently, lead to spin relaxation (**Figure 2a**). For example, although previous studies[18,70] suggested that the DP mechanism should be negligible for spin flip along the out-of-plane direction in monolayer TMDs as the mirror symmetry with respect to the plane of transition metal atoms secures a zero out-of-plane crystal magnetic field, making the out-of-plane component of the electron or hole spin conserved, the mirror symmetry can still be broken by extrinsically factors, such as the surface roughness of the substrates. This gives rise to a Rashba SOC and a p-dependent effective magnetic field with in-plane components,[18] thus opening scattering channels as described by the DP mechanism. Several theoretical works have demonstrated that the DP mechanism dominates conduction band electron spin relaxations in monolayer TMDs by intravalley scattering at cryogenic temperature. As the temperature increases, intervalley scattering becomes more important.[67,70,71] The typical calculated τ_s for electrons is in the order of hundreds of picoseconds to nanoseconds at a low electron density region (Figure 2b) and decreases with higher electron concentration,[70] agreeing with experimentally observed results.[30,65] Interestingly, a similar carrier density dependence on exciton valley dynamics is observed in excitation power-dependent measurements in monolayer WSe_2, suggesting that the DP mechanism may also play a role in exciton valley depolarization, although minor compared to electron-hole exchange interactions.[72] For valence holes near the K/K' point of the Brillouin zone, spin relaxation by the DP mechanism is significantly suppressed due to the large valence spin band splitting, reaching up to 100 meV in monolayer TMD systems. The small fluctuating effective (Rashba) magnetic fields do not provide enough energy for a spin flip within the same valley.[73,74]

2.2.2. Elliot-Yafet (EY) Mechanism

The Elliot-Yafet (EY) mechanism involves spin relaxation during a momentum scattering event by phonons or impurities. Because of the strong SOC, the spins for electrons and holes are not pure spin states anymore. Therefore, every time the carriers are involved in a scattering event, for example, by lattice vibration (phonons) or local defects, they have the chance to couple to a different spin state (Figure 2c). In typical semiconducting systems like monolayer TMDs, the typical electron spin relaxation time governed by the EY mechanism is calculated to be orders of magnitude longer than that described by the DP mechanisms[70,73] primarily because of the marginal spin mixing,[70] which makes the EY mechanism negligible during electron spin relaxation processes in TMD materials. However, since the DP scattering channel is inhibited in hole spin relaxation processes, the EY mechanism can be important in determining hole spin lifetime,

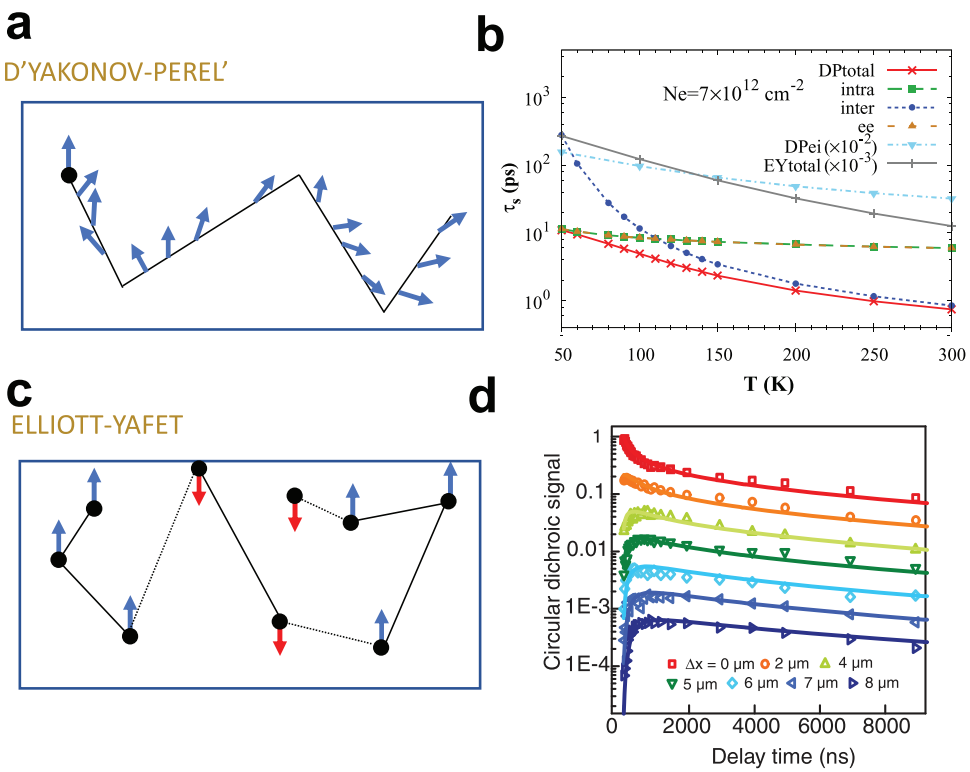

Figure 2. a) Illustration of DP mechanism. The effective magnetic field due to SOC leads the spin to precess during any momentum scattering and causes the spin state to flip. b) Total in-plane spin relaxation time of conduction band electrons in monolayer MoS_2 due to the DP mechanism and that calculated with only the intravalley or intervalley process included as a function of temperature T with an electron density of 7×10^{12} cm^{-2}. In comparison, the EY mechanism plays a minor role here due to a much longer spin relaxation time scale. Reproduced with permission.[70] Copyright 2014, American Physical Society. c) Illustration of EY mechanism involving spin flip caused by electron-phonon or electron-defect scattering. d) Decay dynamics of the pure spin-valley diffusion current at different distances from the origin. The valley lifetime of $\tau = 20$ μs can be extracted via data processing. Reproduced with permission.[6] Copyright 2018, American Association for the Advancement of Science (AAAS).

which is expected to be dominated by phonon-assisted intervalley spin scattering.[74] A recent theoretical paper based on the ab initio density-matrix approach also calculated a hole valley depolarization lifetime on the order of microsecond.[73] Experimental works using the pump-probe method to image the diffusion of valley polarized holes in WS_2-WSe_2 heterostructure observed a valley lifetime of ≈20 microseconds at 10 K, which is also controllable through electrostatic gating[6] (Figure 2d). Similar results have also been reported in WSe_2/MoS_2 heterostructure via photo-induced circular dichroism (CD) spectroscopy.[66] These findings make valley-polarized holes promising candidates for realizing spintronic and valleytronic devices.

As mentioned earlier, phonons are a main source of spin flipping in the EY mechanism. In monolayer TMD systems, coherent acoustic phonons at the K-point of the Brillouin zone are believed to effectively mediate the valley transfer of carriers.[75–78] Density functional theory (DFT) results[75] show that electrons at conduction band minimum at K points are most strongly scattered by longitudinal acoustic (LA) phonons, while K point holes interact most strongly with transverse acoustic (TA) phonons. Optical E' and A_1 phonon modes also contribute finitely to the total scattering process, while the remaining optical E'', A_2'' and out-of-plane acoustic (ZA) phonon modes are found to be negligible due to the weak coupling.[78] A recent study shows that the hole-phonon coupling strengths in the spin-split valence band states at K point in monolayer TMDs are very different. Holes in the upper band are expected to have a very long lifetime, while holes in the lower band are strongly affected by phonon scattering.[76] As the strong spin-orbit interaction in monolayer TMD systems favors a hole population in the upper band at K point without a significant number of carriers in the lower band, the overall spin relaxation time for holes is long even at room temperature.[76] Notably, the hole mobility in monolayer TMDs is predicted to be comparable to bulk silicon,[75] offering attractive alternatives to conventional semiconductors in electronic applications with nanometer dimensions.

2.3. Extrinsic Valley Scattering by Defects

Defects in materials break the translational symmetry and can mediate intervalley scattering and valley relaxation.[79–81] To understand the impact of different defects on valley dynamics, let us take graphene without bandgap or SOC as a simple model. According to the relative position between Fermi level and Dirac point in the energy band, a vacancy can be categorized into two types, namely neutral defects and charged defects, as illustrated in **Figure 3a**. When the Fermi level is above the Dirac point, the resonance state is populated and forms the neutral defect.

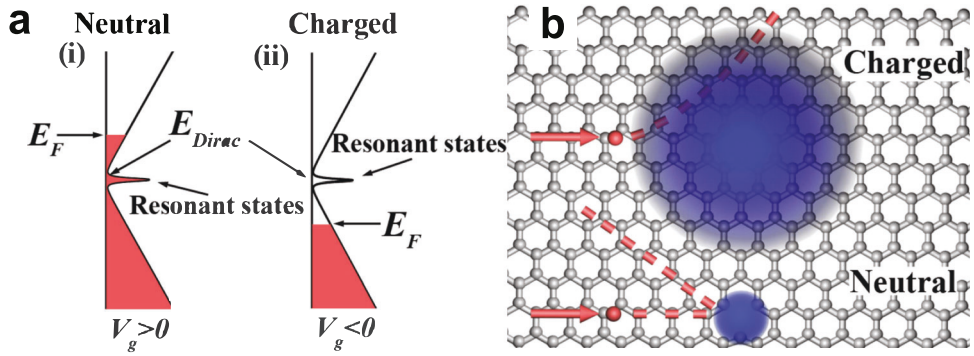

Figure 3. a) Density of states of neutral and charged states of defects: i, defects are neutral as Fermi level in conduction band; ii, defects are charged as Fermi level in valence band. b) The scattering mechanisms of neutral and charged defects differ markedly. In instances where impurity states are populated, defects remain electrically neutral with short-range interaction, causing strong intervalley scattering. Conversely, when impurity states are unpopulated and defects acquire a charged state, a long-range Coulomb potential effectively screens the short-range potential and suppresses intervalley scattering. Reproduced with permission.[82] Copyright 2016, APS.

Conversely, a charged defect appears when the Fermi level is below the Dirac point.[82]

Figure 3b shows the mechanism of carrier scattering in neutral and charged defect states. In neutral states, carriers encountering these defects scatter predominantly via short-range potentials, thereby exhibiting strong intervalley scattering and the phenomenon of weak localization. On the contrary, in charged defect states, carrier transfer is primarily governed by the long-range Coulomb potential, with few carriers capable of penetrating the Coulomb field to undergo intervalley scattering via short-range potentials, so the dynamics of valley relaxation are suppressed, a phenomenon that finds experimental validation in magnetoconductivity and transport experiments. The same phenomenon of charge-state controlled scattering is generally applicable to band insulators with in-gap defect states, as previously shown in various semiconductors.[83–85] Clearly, the introduction of long-range potentials to suppress intervalley scattering holds immense promise for advancing the field of valleytronics.

Surprisingly, in some cases defects may instead stabilize spin-valley polarization. For example, sulfur/selenium vacancies in TMDs are the most common point defects and are thought to trap excitons to form quantum-dot-like localized states that emit below the energy of the neutral excitons. First-principle calculations and time-resolved photoluminescence (PL) spectroscopy of monolayer WSe_2 reveal that selenium vacancy-bound excitons exhibit a long recombination lifetime of 200 ns and robust valley polarization with a lifetime exceeding 1 μs.[86] This phenomenon is intricately linked to the presence of multiple defect bands in the band structures, as the density functional theory calculations indicate that selenium vacancies generate two additional unoccupied bands and one occupied band, which has different influences on the spin-valley coupling and recombination dynamics. Considering the exchange interaction mechanism of intervalley scattering, bound excitons should not have such a long valley lifetime. Therefore, it is possible that only the long-lived polarized holes are trapped until recombined with a diffusing free electron to emit polarization-conserved photons. Regardless of the microscopic mechanism, defect engineering is a potential approach to tailor the optical response of valleytronic materials.

Furthermore, graphene domain walls serve as a fascinating platform for probing valley physics. In contrast to valley mixing induced by atomic defects at graphene edges, domain walls between AB- and BA-stacked bilayer graphene exhibit chiral boundary states of quantum valley Hall insulators.[79] Smooth domain walls preserve the electron valley index, giving rise to distinct topological phases with opposite valley properties under similar vertical electrical fields. External electric fields can modulate the bandgap in bilayer graphene, allowing valley-polarized electrons to traverse domain walls in gapped bilayer graphene, with electrons in K/K' valleys moving in opposite directions. Notably, the electron mean free path along smooth domain walls far exceeds that within the domains in bilayer graphene, underscoring the topological protection supported by chiral electronic modes. Importantly, intervalley scattering from smooth domain walls can be effectively neglected, highlighting the robust nature of chiral valley channels along domain walls in AB- and BA-stacked graphene architectures.

2.4. Ultrafast Control of Valley Polarization

Although excitons have limited valley lifetime, they may still be valuable if the information can be processed and read in a shorter timescale. Using a femto-second pulsed laser as an external stimulus has been proved to be an effective method to manipulate material properties in ultrafast timescale.[87,88] Indeed, recent investigations on WSe2 have revealed that the optical generated excitons in one single valley can be transferred into the opposite one by an intense multi-cycle Terahertz (THz) field within sub-cycle timescale, proved by the elliptical polarization emission in the high-order sideband generation spectroscopy and DFT calculations.[89] Similarly, another work reported the manipulation of valley pseudospin via the optical Stark effect in monolayer WSe_2, using a circular polarized gate pulse with the energy slightly below the bandgap[90] (**Figure** 4a–c). Here, the circularly polarized pulse serves as an effective d.c. magnetic field that breaks the time-reversal symmetry and thus lifts the energy degeneracy of K and K' valleys. The induced change in the transition energy of the two valleys gives rise to different oscillation

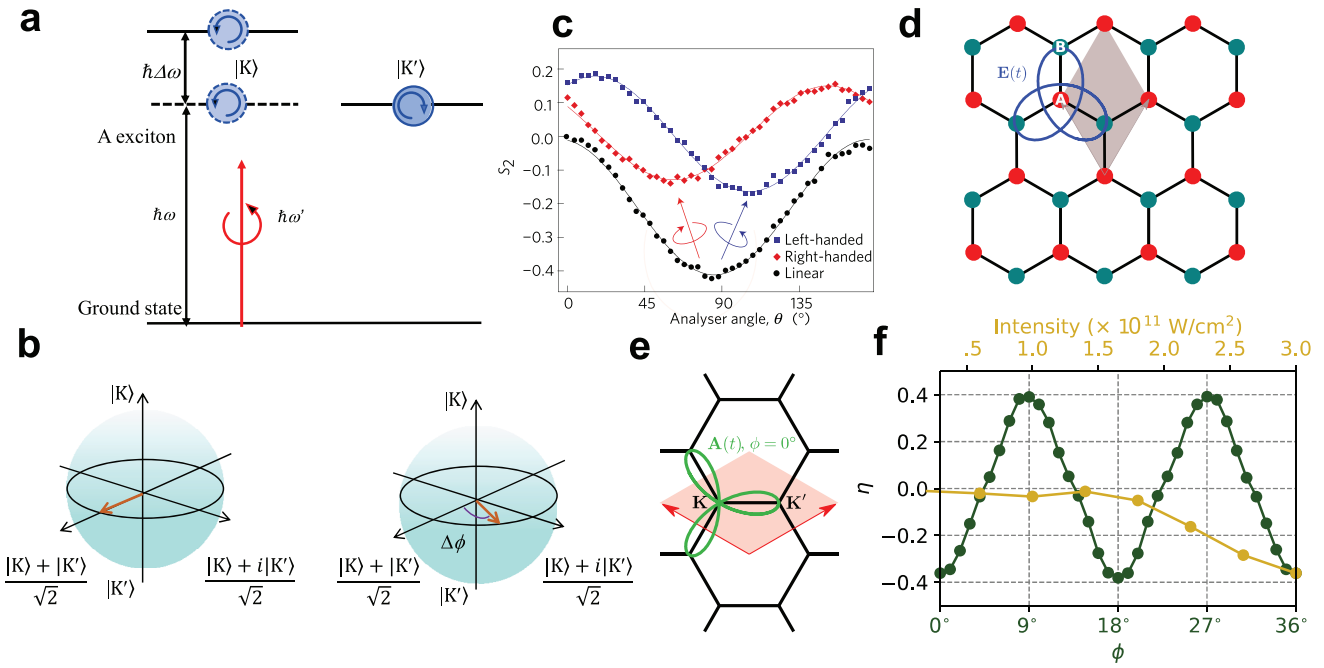

Figure 4. a,b) Illustration of the optical Stark effect. A linear polarized pulse will excite the excitons having coherent superposition in the K and K′ valleys with a fixed phase relationship. When a strong left-circularly polarized control pulse of below-gap radiation is applied (solid red arrow), the exciton transition energy in the K valley is increased by $\hbar\Delta\omega$. While the control pulse is present, a dynamic phase difference $\Delta\varphi$ develops between the exciton components in the two valleys. The pseudospin in the Bloch sphere is correspondingly rotated by an angle $\Delta\varphi$, just as would occur for an out-of-plane magnetic field (open arrow). [c) The rotation of the valley pseudospin is determined by the orientation of the polarization of the photoluminescence measurements. Reproduced with permission.[90] Copyright 2017, Nature Portfolio. d) Lattice structure with the Lissajous draw of the bicircular electric field breaking the structural symmetry. Reproduced with permission.[91] Copyright 2021, OPTICA. e) Optical induced asymmetry in the momentum space. Reproduced with permission.[91] Copyright 2021, OPTICA. f) Asymmetry in the populations in the conduction band as a function of phase difference of two fields ϕ (green line with an intensity 3×10^{11}W cm^{-2}) and laser intensity (yellow line with $\phi = 0°$). Reproduced with permission.[91] Copyright 2021, OPTICA.

frequencies for excitons at K and K' valleys, which develops a dynamic phase difference $\Delta\varphi$. Such phase evolution can be described as a rotation in the Bloch sphere of valley pseudospin which can be revealed by the PL spectra. Further time-resolved pump-probe measurements indicate that the rotation is maximized when the gate pulses are applied within ≈50 femtoseconds after exciton injection and disappears when the delay exceeds 800 femtoseconds, which indicates that the coherence lifetime is smaller than the typical exciton valley population lifetime.

Ultrafast optical control also offers new insight to realizing valleytronics in pristine graphene. As demonstrated by Mrudul et al,[91] valley selective excitation and valley selective high harmonic generation can be achieved in pristine graphene when it is pumped by a combination of two counter-rotating circularly polarized fields simultaneously, one in fundamental frequency and another in second harmonic frequency, as shown in Figure 4d–f. The existence of such a bicircular field breaks the inversion symmetry of the crystal and by tuning the relevant phase difference between two pulses, one can select the valleys where the electron–hole pairs and higher-order harmonics are generated. The tunable inversion asymmetry provides a means to access excitation probabilities induced by the same field in different valleys. This work presents a milestone in advancing valleytronics in 2D monolayer materials with zero Berry curvature.

3. Novel Materials for Valleytronics

The main problem with monolayer TMDs and graphene for scalable valleytronic applications comes more from the practical aspects than the lack of fundamental principles or ideal performance. For example, transport properties of monolayers are inherently susceptible to crystalline and fabrication imperfections; due to small interaction length, the light-valley conversion needs to be enhanced by external optical cavities; the symmetry breaking or energy splitting is not large enough to suppress intervalley scattering at elevated temperatures, etc. From our discussion above, the ideal material should combine a few properties: few-layer or bulk; large SOC; small electron-phonon coupling; easy electron-hole separation; defect-free or having reproducible defect properties. To this day, robust valley polarization has been found in many other materials. However, there is not yet a perfect material with all these properties, which have kept researchers expanding their search into a diverse range of systems from 2D hexagonal lattices to non-hexagonal lattices and heterostructures. **Table 1** summarizes the new valleytronic materials and their properties compared with some of the highest-performed TMD materials to the best of our knowledge. It may not be an exhaustive or up-to-date list, but contains good representatives of the possible strategies to enhance valleytronics.

Table 1. Summary of representative valleytronic TMDs, graphene, and novel valleytronic materials.

Materials	Thickness	Valley carriers	Method	Experimentally demonstrated performance	Theoretically predicted properties
Electron irradiated WSe_2	Monolayer	Excitons	(Exp.) Photoluminescence	30% valley polarization and >1 µs valley lifetime (at 5 K)[86]	–
$MoTe_2$	Monolayer	Trions	(Exp.) Photoluminescence	33% valley polarization and >0.9 ns valley lifetime (at 4 K)[92]	–
WSe_2/MoS_2	Monolayer/ Monolayer	Holes	(Exp.) Photoluminescence	Nearly 100% valley polarization and >40 µs valley lifetime (at 10 K)[66]	–
Silicene	Monolayernano-ribbons	Free carriers	(Theory) Low-energy effective Hamiltonian	–	Quantum spin Hall-quantum anomalous Hall insulators[93,94]
$BiAsI_2$	Monolayer	Photo-carriers	(Theory) First-principles calculations	–	Gate-induced valley switching[86]
Germanene	Monolayer	Photo-carriers	(Theory) First-principles calculations	–	Gate-induced valley switching[86]
Graphene	Bilayer double quantum dots	Valley triplet	(Exp.) Charge transfer with valley blockade	Lifetime >500 ms (at 50 mK)[32]	
	Trilayer	Free carriers	(Exp.) Anomalous Hall effect	Valley-polarized "quarter-metal" phase (at 5.6 K)[95]	–
$MoSi_2As_4$	Monolayer	Photo- and free-carriers	(Theory) First-principles calculations	–	Spin and Valley Hall effects[96]
$Cs_3Bi_2I_9$ (CBI)	Odd number, up to 11 layers	Excitons	(Exp.) Photoluminescence	30% valley polarization (at 83 K)[97]	–
Cr_2COF	Monolayer	Free carriers	(Theory) First-principles calculations	–	Valley energy splitting of 334 meV[98]
TiSiCO	Monolayer	Free carriers	(Theory) First-principles calculations	–	Gate-induced valley splitting ≈100 meV[99]
$BaMnSb_2$	Bulk single crystal	Free carriers	(Exp.) ARPES and Quantum Hall effect	Spin-valley locking with 0.35 eV spin splitting (at 50 K)[100]	–
CBI/$MoSe_2$ heterostructures	Five layer /Monolayer	Interlayer excitons	(Exp.) Photoluminescence	Exciton lifetime of ≈250 ns (at 10 K)[101]	–

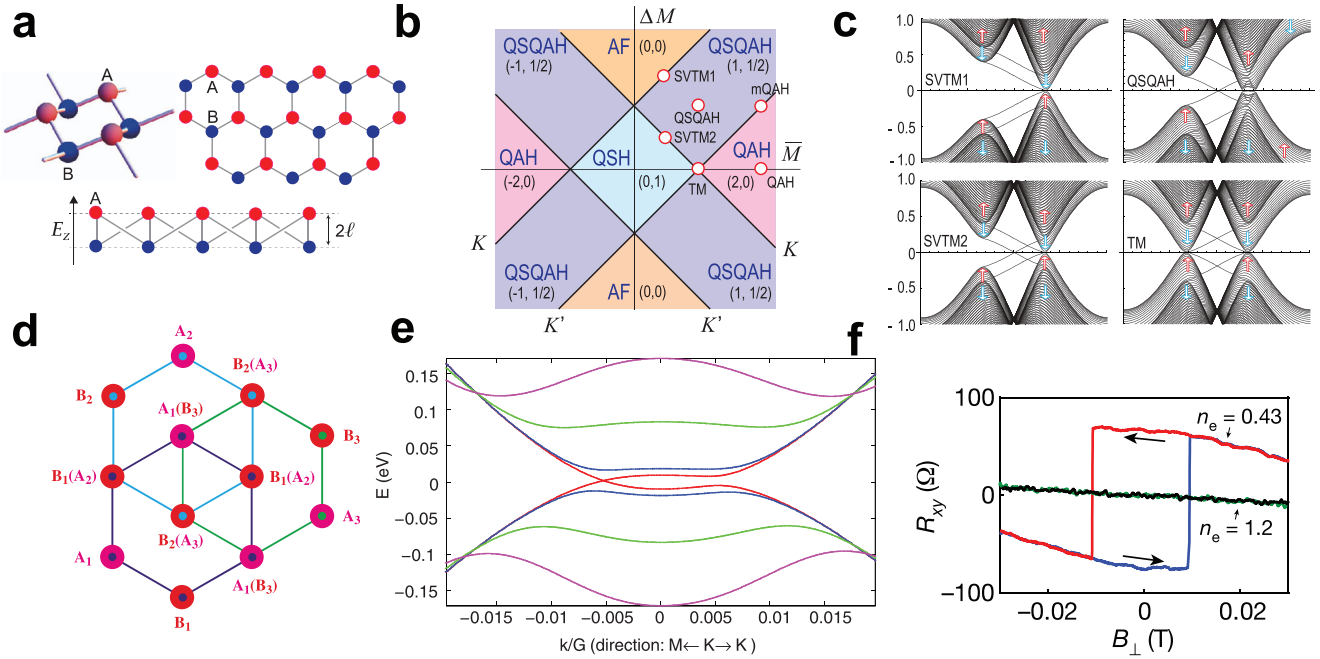

Figure 5. a) Crystal structure of silicene. Reproduced with permission.[105] Copyright 2012, IOP Science. b) Phase diagram of silicene as a function of an external staggered exchange field ΔM and mean exchange field $\bar{M}$. Reproduced with permission.[93] Copyright 2013, American Physics Society. c) The silicene nanoribbon band structure at K and K' points under different quantum phases denoted in b). Reproduced with permission.[93] Copyright 2013, American Physics Society. d) Lattice structure of ABC-stacked graphene trilayer; blue/cyan/green indicate links on the top/middle/bottom layers while purple/red distinguish the A/B sublattices. Reproduced with permission.[113] Copyright 2010, American Physics Society. e) The band structures of ABC graphene trilayer with external electric potential differences between the outermost layers. The external potential difference values are 0.0 (red) eV, 0.2 (blue) eV, 1.0 (green) eV, and 2.0 (magenta) eV, respectively. G is the length of the reciprocal vectors and k = 0 is a K point. Reproduced with permission.[113] Copyright 2010, American Physics Society. f) Low-magnetic-field Hall resistivity measured at two values of carrier density, representing half- (black line) and quarter- (red and blue lines) metal phases. A hysteretic anomalous Hall effect is observed in the valley-polarized quarter-metal, but not in the valley-unpolarized half-metal. Reproduced with permission.[95] Copyright 2021, Nature Portfolio.

3.1. Monolayer Allotropes with Strong Spin Orbit Coupling

Increasing SOC with heavier elements can potentially extend valley lifetime. For example, Silicene offers possible avenues for valleytronic compared with monolayer graphene due to its distinct buckled geometry (**Figure 5a**).[102,103] It shares a similar hexagonal lattice structure as graphene, but unlike graphene whose planar geometry and subsequent gapless band structures prevent exciton-based valleytronics, the larger Si-Si bonding distance in silicene weakens the π-π orbital overlaps, resulting in buckled structures with sp3 hybridization. This unique structure opens a bandgap at the Dirac points, driven by strong SOC.[93,103–105] It is found that the low-energy electronic states of silicene can be described by Dirac equation with relatively large spin-orbit interactions and is controllable by an out-of-plane electric field.[106] Theoretical investigations have further demonstrated that the introduction of a staggered exchange field can induce diverse phase diagrams in silicene, as illustrated in Figure 5b.[93] Of particular interest is the emergence of a novel topological state known as the quantum spin–quantum anomalous Hall (QSQAH) insulator in silicene nanoribbons. In this state, the quantum anomalous Hall (QAH) effect is realized at the K point, while the quantum spin Hall (QSH) effect manifests at the K' point, as depicted in Figure 5c. Alternatively, under different conditions, silicene may adopt a single-valley topological metal (SVTM) semimetal state, leading to phenomena such as the opening or closing of the bandgap at the K or K' point while preserving spin degeneracy. The distinctive spin valley structures of these states may be revealed by spin-valley-selective circular dichroism, but there is not yet any experiment due to the challenge of polarization-dependent spectroscopy in materials at deep subwavelength scale. Additionally, another very recent theoretical work has also demonstrated the valley-polarized photocurrent switch based on circular bulk photovoltaic effect in monolayer hexagonal $BiAsI_2$ and germanene.[94]

3.2. Multilayer Stacks with Strong Electron Correlation

Valleytronics can be realized in gapless systems when the gap is opened by stacking-enabled electric-field control or strong electron correlation. Unconventional valley-dependent optical selection rules and valley-selective Hall effect (VHE) was recently observed in bilayer graphene.[107,108] In VHE experiments, the sign of the anomalous Hall conductivity is controlled by the helicity of the incident light, which excites free carriers in a specific valley due to optical selection rules. The anomalous Hall velocity is caused by the valley contrasting Berry curvature in materials with no inversion symmetry. Without optical excitations, there is no net charge current, but valley polarized free carriers will accumulate at the edge of the device, and thus can transport information without the additional energy cost of charging

parasitic capacitors in the circuit.[109,110] Another way to create valley states in bilayer graphene is through gate-controlled double quantum dots.[32] Depending on the geometry, magnetic field, and the gate voltages, the ground state of two electrons can be toggled between state (1,1), one electron in each dot with spin and valley triplet, and state (0,2), two electrons in one dot with spin triplet and valley singlet. The (1,1) state is initially prepared as the ground state, and then lifted above (0,2) state to allow energy relaxation. The lifetime of (1,1) is thus determined by the charge tunneling lifetime, which is negligibly short in this case, and the valley flipping lifetime from triplet to singlet, which is the limiting step and found to be over 500 ms, even longer than the spin lifetime (<60 ms). Such a long lifetime can be understood by the lack of scattering from large-momentum phonons or defects at an extremely low temperature of 50 mK, showcasing the potential advantage of completely electromagnetically neutral valleytronics over spintronics in certain conditions.

The robust valley polarization may be extended to bulk states in trilayer graphene exhibiting various stacking sequences.[111,112] Among these configurations, rhombohedral ABC-stacked trilayer graphene (Figure 5d) stands out due to its intriguing physics, especially unconventional superconductivity.[111] In ABC-stacked graphene trilayers, the low-energy band is nearly flat with a cubic dispersion at the two inequivalent K and K' points, attributed to strong interlayer interactions. The valence and conduction bands touch at the Fermi level in the absence of an external field, with the presence of nearly flat bands near the Fermi level. Upon the application of an external field, a direct energy gap is observed at the K and K' states (Figure 5e).[113] Remarkably, Zhou et al. reported a series of novel phases in ABC-stacked graphene trilayers modulated by doping level and electric field. Among these phases, a spin- and valley-polarized "quarter-metal" phase was identified and detected via low-magnetic-field Hall resistivity measurements (Figure 5f).[95] The spontaneous valley polarization can potentially be switched by external optical fields or carrier injections, especially near the critical point, and thus may enable strong nonlinearity and opens new possibilities for valleytronic transistors.

3.3. New 2D materials with Hexagonal Lattices

Materials beyond TMD can improve valleytronics in the following ways: multilayer for high conversion efficiency; chemical stability and low defect levels; non-degenerate valleys. Apart from graphene, TMDs, and their derivatives, the exploration of novel vdW materials with hexagonal lattices have also been predicted and pursued to broaden the family of valleytronic materials for potential applications. The MA_2Z_4 family presents an intriguing avenue, offering tunable bandgap from a large number of choices in the M (transition metals), A (group IV), and Z (group V), as well as from the sensitivity to strain. In 2020, pioneering research conducted by Hong et al. experimentally synthesized monolayer $MoSi_2N_4$ and showed they may exhibit better stability against oxidation than MoS_2 in ambient conditions, hot water, and high temperatures.[114] Following the work, Li et al.[96] predicted the emergence of valley degrees of freedom in MA_2Z_4, such as $MoSi_2As_4$, which has a direct bandgap at the K point according to first-principles calculations (**Figure 6a**). Similar to monolayer TMDs, the valleys exhibit spin-valley coupling and Berry curvature (Figure 6b). Calculations found among MA_2Z_4 significant variations in the size of the direct bandgap, and in some cases the indirect bandgap between the K point and the Γ point. Moreover, the type of gap is tunable by biaxial strain, while the optical selection rule is very robust near the valleys (Figure 6c).

Although vdW monolayers have important advantages for devices, such as being structurally simple and field-tunable, they are also sensitive to the ambience and only capture a small fraction of incident light without enhancement from photonic cavities. Recently, Liang et al.[97] demonstrated valley polarizations in multilayers of perovskite derivative materials directly synthesized by chemical vapor deposition (Figure 6d,e). Polarization-resolved second harmonic generation revealed that odd-layered $Cs_3Bi_2I_9$ break inversion asymmetry, and polarization-preserved photoluminescence was observed for sample thickness up to 11 layers $Cs_3Bi_2I_9$, indicating robust SOC-protected valley carriers. First-principles calculation verified the unique optical and electronic properties of this perovskite derivative, attributing the high degree of valley polarization and large optical absorption to its parallel bands at the K points (Figure 6f). The newly established principle for materials selection is less dependent on thickness and thus may enable more scalable valleytronic applications.

Introducing ferromagnetism has emerged as an effective approach for achieving tunable valley splitting, thereby extending the valley lifetime. Such examples include Co-doped MoS_2[115] and $MoTe_2$/EuO heterostructure,[116] but these materials often face challenges such as low Curie temperatures and impurity scattering, limiting their practical utility. An important step toward higher Curie temperatures was made by Li et al. in 2021, predicting that 2D MXenes with hexagonal lattices exhibit asymmetric structures upon surface functionalization.[98] This surface modification breaks the inversion symmetry, resulting in valley polarizations with multiple possible magnetic orders, including ferromagnetism, ferrimagnetism, and antiferromagnetism, as depicted in Figure 6g,h. For valleytronic properties, Cr_2COF MXenes[117] are promising due to their high Curie temperatures, robust valley polarization, and large valley splitting energy of 334 meV. The spontaneous spin polarization at the valley points was visualized by Berry curvature calculations (Figure 6i). By band structure analysis, diverse MXene structures can be tailored to explore the intricate relationship between valley degrees of freedom and spin. However, the utilization of 2D magnetic MXenes in valleytronics is still challenging due to the difficulty in synthesizing high-quality crystals with specific engineered structures, as the replacement of functional groups directly influences magnetism. Elevated annealing conditions can lead to the exchange or disruption of functional groups such as OH or F, complicating the synthesis process. Therefore, future research needs to prioritize the synthesis of 2D MXenes with controlled type and concentration of functional groups for enhancing valleytronic properties. Theory also predicted transition metal halides H-ZrX2 (X = Cl, Br, I)[118] doped with chromium (Cr) with large valley Zeeman splitting. Monolayer ZrX_2 exhibits a pair of degenerate valleys at the K and K' points in the valence band maximum and the conduction band minimum with finite spin-orbit splitting. With Cr-doping, ZrI_2 exhibits a valley splitting of 108 meV, corresponding to an effective Zeeman magnetic field of 778 T,

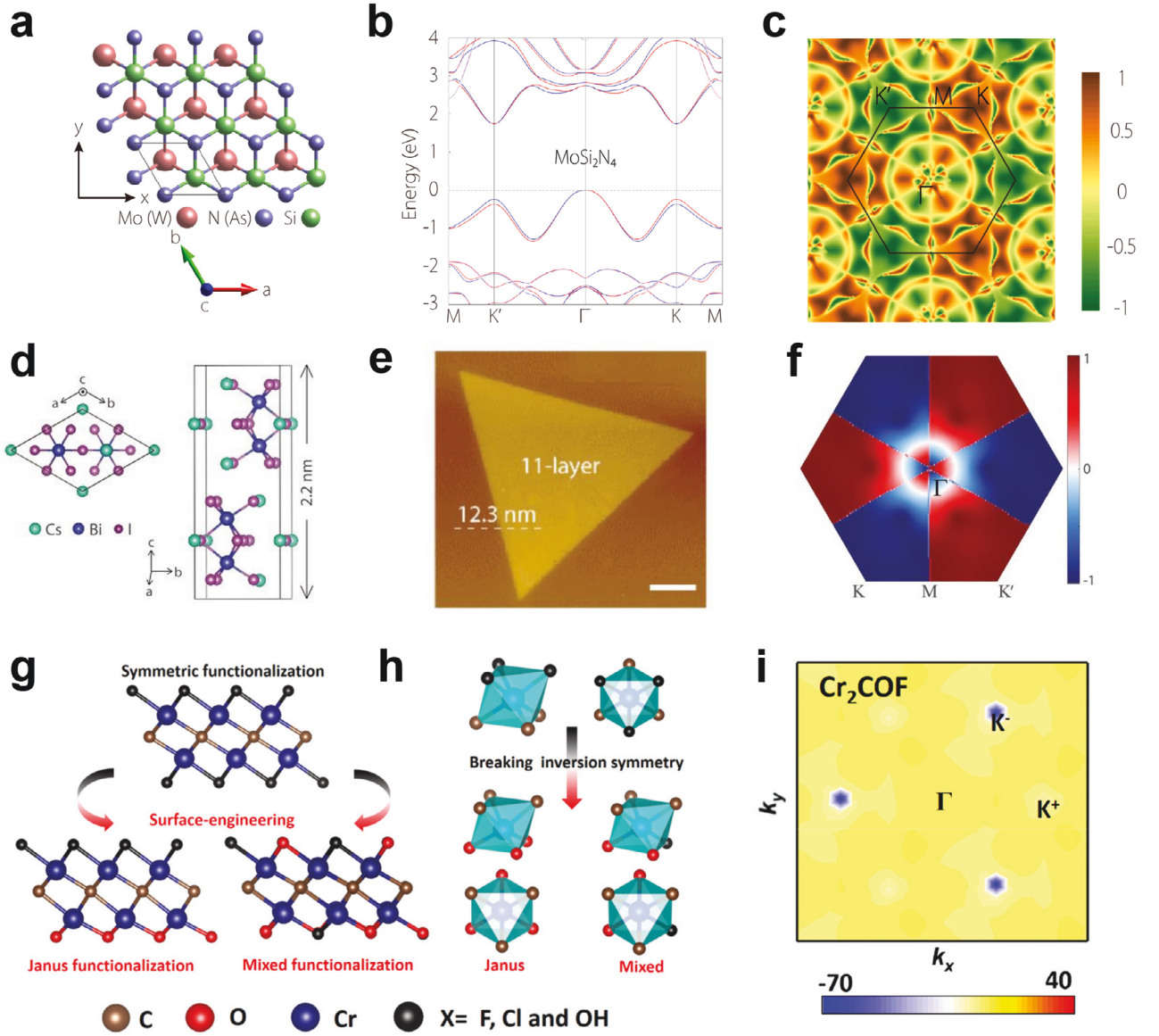

Figure 6. a) Crystal structures of the MA_2Z_4 family. Reproduced with permission.[96] Copyright 2020, American Physics Society. b) Band structure of monolayer $MoSi_2As_4$ in the presence of the SOC effect. Red and blue indicate the spin-up and spin-down bands, respectively. Reproduced with permission.[96] Copyright 2020, American Physics Society. c) The circular polarization of $MoSi_2As_4$ calculated for transitions between the highest valence band and lowest conduction band. Reproduced with permission.[96] Copyright 2020, American Physics Society. d) Crystal structures of $Cs_3Bi_2I_9$ from top and side views, respectively. Reproduced with permission.[97] Copyright 2020, Wiley. e) AFM images and corresponding height profiles of $Cs_3Bi_2I_9$ flakes with the thickness of ≈12.3 nm, which correspond to the 11-layer sample. The scale bar in e is 5 µm. Reproduced with permission.[97] Copyright 2020, Wiley. f) the calculated momentum-resolved valley polarization of monolayer $Cs_3Bi_2I_9$ with SOC. The optical transition in a large vicinity of the K and K' points maintains high helicity close to −1 and 1, respectively. Reproduced with permission.[97] Copyright 2020, Wiley. g) Symmetric and asymmetric MXene functionalization. h) A scheme showing the inversion symmetry breaking for Janus and mixed-functionalized Cr_2C MXenes. i) Berry curvatures of Cr_2COF in the full Brillouin zone. Reproduced with permission.[98] Copyright 2021, RSC Publishing.

strongly suppressing intervalley scattering even at elevated temperatures.

3.4. Non-Hexagonal Materials

From the valley manipulation aspect, the valleys in hexagonal structures are connected by time reversal, which can be manipulated by magnetic fields, circularly polarized optical fields, or current.[48,54,119,120] But such tuning methods are not always applicable. By contrast, materials with other symmetry types may enable new manipulation mechanisms easier to implement. To switch valley energy-efficiently via electrostatic gating, Yu et al.[99] have developed a novel mechanism, named valley layer coupling, where two valley polarizations are also distinguished by the vertical location of electrons and holes, enabling a direction

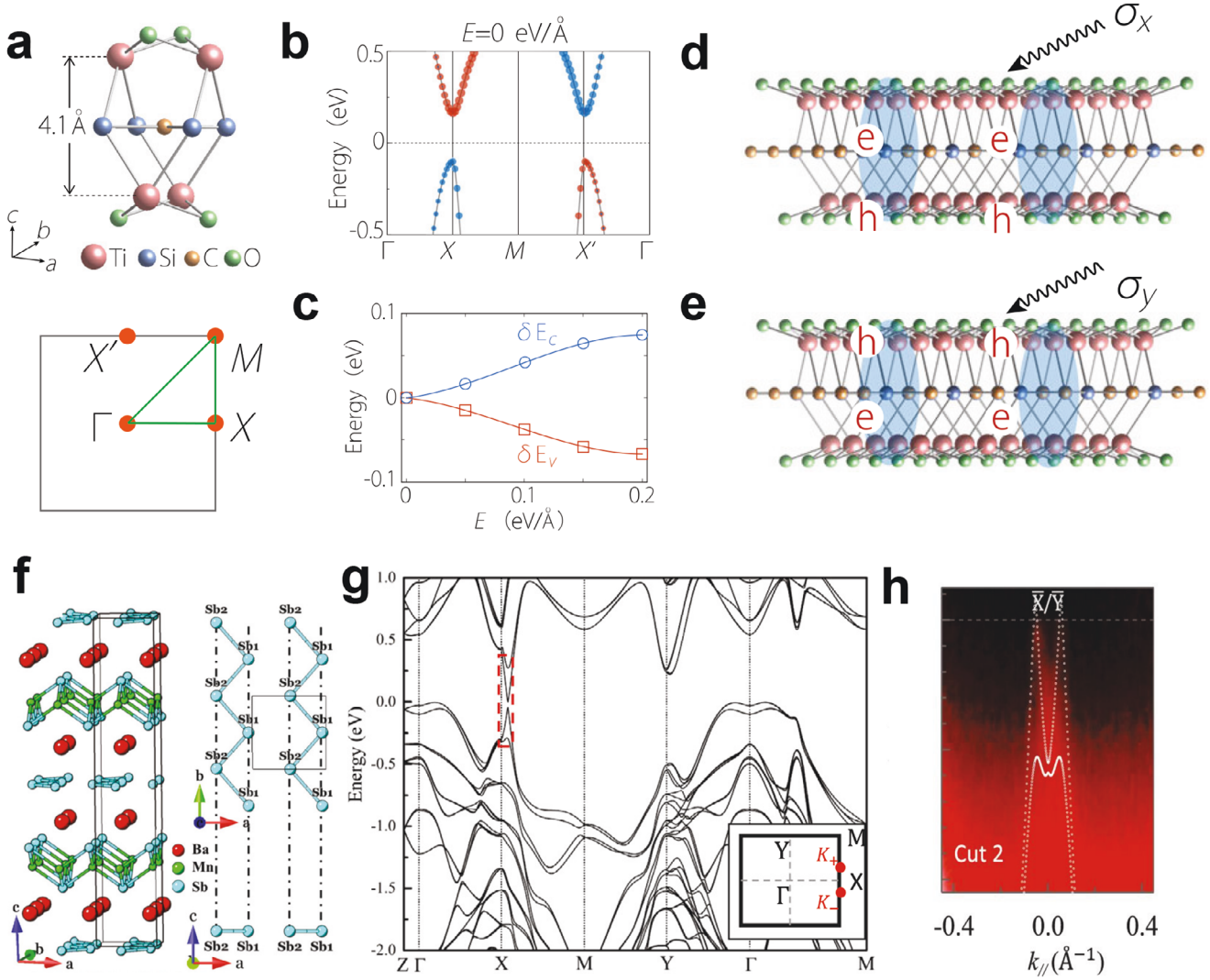

Figure 7. a) The crystal structure of a monolayer TiSiCO and corresponding Brillouin zone. Reproduced with permission.[99] American Physics Society. b) The band structure of a monolayer TSCO. Reproduced with permission.[99] American Physics Society. c) Valley splitting of valence band and conduction band modified by out-of-plane electrical field. Reproduced with permission.[99] American Physics Society. d,e) linear polarized optical field σ_x and σ_y induced valley polarization at the X and X' points. Reproduced with permission.[99] American Physics Society. f) The schematic of the *I*2 mm crystal structure of $BaMnSb_2$. Reproduced with permission.[100] Copyright 2021, Nature Portfolio. g) The band structure from the first-principles calculation. Inset shows the first BZ, and the red dots label the two gapped Dirac cones at $K_{\pm}$. Reproduced with permission.[100] Copyright 2021, Nature Portfolio. h) Comparison of the calculated band (dotted lines) and the band probed by ARPES along MX line. Reproduced with permission.[100] Copyright 2021, Nature Portfolio.

coupling between valley and external gate field as illustrated in **Figure** 7a. The work predicted a monolayer TiSiCO with square lattice, whose Brillouin zone is also square, in which the conduction band and valence band extrema occur at the X and X' points in Figure 7b. This principle provides a continuous control of valley energy splitting in a wide range as depicted in Figure 7c. More importantly, the square lattice of TiSiCO offers linearly polarized optical selection rules for the inequivalent valleys from Γ-X and Γ-Y valleys, similar to the valley-selective linear dichroism which was experimentally demonstrated in layer thin film Tin sulfide (SnS),[121] but with an additional protection against intervalley scattering from the opposite dipole moment of excitons (Figure 7d).

Another example is bulk crystals of $BaMnSb_2$, a Dirac semimetal gapped by lattice distortion with a layered orthorhombic structure (*I*2 mm) (Figure 7e), breaks the inversion symmetry according to second harmonic generation and neutron scattering.[100] The combination of inversion symmetry breaking and SOC in $BaMnSb_2$ resulted in a spin-valley locking. $BaMnSb_2$ exhibited a similar spin splitting of ≈0.35 eV in both conduction and valence bands, unlike monolayer TMDs, where the conduction band SOC has a range of 10 s of meV and the valence band SOC is much larger between 0.15 and 0.5 eV. Notably, the energy gap of Dirac cones in $BaMnSb_2$ was ≈50 meV as measured by angle-resolved photoemission spectroscopy (ARPES), which is pushed by SOC to be much smaller than the initial

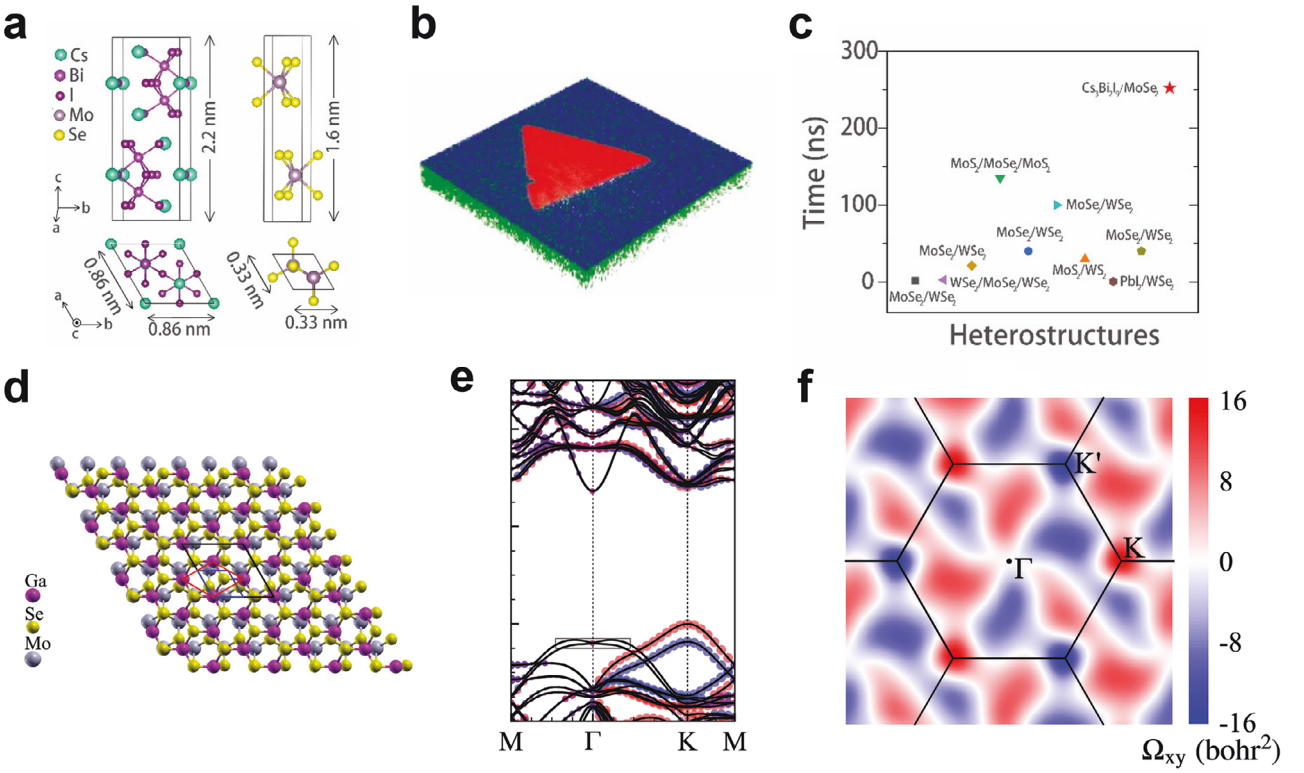

Figure 8. a) Crystal structures of $Cs_3Bi_2I_9$ and $MoSe_2$ from top and side views, respectively. Reproduced with permission.[101] Copyright 2023, Elsevier. b) 3D ToF-SIMS image of a $Cs_3Bi_2I_9/MoSe_2$ vdW heterostructure, including the $Cs_3Bi_2I_9$ layer (red triangle), the $MoSe_2$ layer (blue part), and the SiO_2 substrate layer (green part). Reproduced with permission.[101] Copyright 2023, Elsevier. c) Comparison of the interlayer exciton lifetime of $Cs_3Bi_2I_9/MoSe_2$ vdW heterostructures with previously reported heterostructures. Reproduced with permission.[101] Copyright 2023, Elsevier. d) The top view of the GaSe/$MoSe_2$ heterostructure. Reproduced with permission.[122] Copyright 2018, American Physics Society. e) Band structure of the GaSe/$MoSe_2$ heterostructure obtained with spin-orbit coupling. The size of the circles denotes the spin projection in the out-of-plane direction, and red and blue indicate positive and negative values, respectively. Reproduced with permission.[122] Copyright 2018, American Physics Society. f) Berry curvature derived by Wannier interpolation. Reproduced with permission.[122] Copyright 2018, American Physics Society.

distortion-induced gap, as shown in Figure 7f,g. Moreover, Liu et al. identified a stacked quantum Hall effect in $BaMnSb_2$, attributed to its layered structure with weak interlayer tunneling. Interestingly, although there exist trivial bands near the Brillouin zone center, the magneto-transport is dominated by the valleys $K_{\pm}$ near the X point, as shown by the nearly perfect half-integer transverse quantum conductance owing to the high mobility near the initial Dirac point. The calculated spin valley degeneracy, equal to 2 according to simulations and experiments, provides solid evidence for the existence of spin-valley locking in $BaMnSb_2$.

3.5. Heterostructures

As previously discussed in Section 2.1, heterostructures with a type-II band alignment are promising candidates for valleytronics because the interlayer excitons in these materials often possess longer lifetime than those of intralayer excitons in monolayers. In a departure from traditional vdW heterostructures based on two TMD materials, Liang et al. recently reported a two-step vapor phase growth process for the creation of high-quality vdW heterostructures comprising 2D $Cs_3Bi_2I_9/MoSe_2$.[101] Unlike TMD heterostructures, $Cs_3Bi_2I_9/MoSe_2$ vdW heterostructure exhibited a large lattice mismatch, leading to reduced overlap of electron and hole wavefunctions (**Figure 8a,b**). Therefore, the type-II heterojunction in the $Cs_3Bi_2I_9/MoSe_2$ vdW heterostructure demonstrated an interlayer exciton lifetime of more than 250 ns, which is the longest reported exciton lifetime to date for valleytronics (Figure 8c). In addition, the large out-of-plane electric field may induce strong Rashba effect in certain vdW heterostructures and influence the spin-valley dynamics.[52] Zhang et al.[122] have theoretically shown that vdW heterostructure based on GaX and MX_2 (M = Mo; X = S, Se, Te) exhibited strong orbital hybridization and Rashba splitting in the valence band around the Γ point, as shown in Figure 8d,e. Orbital-resolved density of state highlighted the pivotal role of p orbitals in Rashba splitting similar to the case of MoS_2/Bi.[123] The in-plane spin splitting from Rashba effect coupled with out-of-plane spin splitting at the K and K' valleys in MX_2 lead to different spin transport paths under external electrical fields, as shown by the complex Berry Curvature map (Figure 8f). Therefore, it is possible to adiabatically manipulate spin states by electric field, a potential route for controlling the valley gate and spin-transfer torque. Furthermore, the tunability of the valence band maximum in the Brillouin zone through both strain and out-of-plane electric

fields introduces an additional degree of freedom for spin-valley manipulation.

4. Conclusion and Outlook

In summary, TMDs helped to make rapid progress in valleytronics, but still face challenges in valley lifetime, materials quality and scalability, and low operating temperatures. All these challenges must be simultaneously solved for practical applications, so the field is still at a very early stage to address them one at a time. The novel valleytronic materials reviewed in this article present potential solutions to the challenges, by features such as larger thicknesses to increase light-matter interaction and larger energy/momentum splitting to reduce scattering rates. Admittedly, these studies are far from complete compared with a decade of research in TMD valleytronics and have not yet proved conclusive advantages of new materials over TMDs. Nevertheless, we believe that each material deserves more systematic research, especially experimental measurements of valley lifetime as a function of temperature, thickness- and size-dependent valley conversion, as well as the sensitivity of performance to defects, either as-grown or introduced during degradation. Although these transport properties are more difficult to predict than the band structures or the presence of valley degree of freedom, new computational tools with the help of artificial intelligence can still help to screen more valley material candidates using good descriptors like SOC, deformation potential, and formation energy.

First, an immediate objective would be to determine and improve the valley lifetime, transport, and operation efficiency of newly predicted valleytronic materials. Such materials may be directly grown by chemical vapor deposition (CVD) or mechanically exfoliated from bulk crystals prepared by chemical vapor transfer. Like the historical development of TMDs, obtaining materials with low defect density is of paramount importance to ensure prolonged valley lifetime, but can be a highly non-trivial task. The challenge becomes even more pronounced when scaling up the production process. While mechanical exfoliation techniques yield pristine micrometer-sized samples, they are inherently low throughput and impractical for industrial applications. To unlock the full potential of valleytronics, large-area growth methods like CVD must be optimized. However, the upscaling of such processes often results in non-uniformity, increased defect density, and grain boundaries, which can hinder the material's performance. Therefore, developing reliable, scalable techniques that can consistently produce wafer-scale 2D materials with minimal defects is essential. This remains a critical bottleneck for their widespread use in real-world applications. Correspondingly, it is also important to develop rapid characterization methods to investigate the structure-property relationships of valley materials to ensure their homogeneity.

Robust valley polarization and long lifetime should not only be shown in extreme conditions like cryogenic temperatures and strong magnetic fields, but eventually also in ambient condition to justify practical applications. The ideal valley carriers may need to combine all the promising valley-stabilizing features in Section 3, e.g., holes with large SOC in a type-II heterostructure with ferromagnetism. Nevertheless, it is difficult to predict whether a material system with all optimal properties exists, and there seems to be no systematic approach to search for it yet. Thus, the continual exploration of the possible materials space for room-temperature valleytronics requires high-throughput, efficient Density Functional Theory (DFT) calculations and experimental feedback, rather than aiming at specific systems by trial and error. Recently, machine learning has been becoming a powerful tool to assist in the design and screening of various functional materials including superconductors, photovoltaic materials, and high entropy alloys. Rather than the conventional paradigm of materials discovery, i.e., identifying a promising materials platform and then exploring synthesis and characterization, it might be the right time to leverage artificial intelligence and machine learning based inverse design to accelerate the development of new valleytronic materials with high performance, structural stability, and a clear synthesis route.[124]

Second, for these new valleytronic materials it is also important to explore novel mechanisms of valley operations for applications like next-generation information devices beyond complementary metal-oxide-semiconductor technology. Generally, beyond optical valley manipulation, electrical, magnetic, and mechanical tuning should also be considered. Electrical tuning leverages gate voltages or electric fields to enable dynamic and reversible manipulation of the potential landscape of excitons and carriers, which is particularly useful in device applications such as transistors and Hall devices. Magnetic tuning, on the other hand, utilizes external magnetic fields or intrinsic magnetic ordering to influence valley polarization, providing a pathway to explore spin-valley coupling and magneto-optic effects in these materials. Mechanical tuning involves strain engineering, where the application of external stress or strain can modify the electronic band structure, thereby affecting the valley properties. It is still an open question whether new materials can offer stronger coupling between valley polarization and the external fields.

For example, the experimental studies of valley polarizations in non-TMD materials (except for graphene) focused on the optical injection of excitons. It is well known that the spin-valley lifetime of free carriers is prolonged compared to that of excitons, but there is not yet any systematic studies of the lifetime of valley polarized free carriers in non-TMD materials. Also, it is well-established that spin-polarized free carriers may be coherently rotated by external fields or spin-orbit coupling, yet the controllable valley switching of free carriers has not been demonstrated, despite the existence of several possible non-optical mechanisms to enable such operations, e.g., gate-confined Coulomb exchange or scattering with valley chiral phonons.[125] Besides valley gates, it is necessary to develop valleytronic devices,[126–129] such as valley transistors, diodes, filters, and detectors. However, only a handful of valleytronic devices were reported to date and in most cases their performance was characterized at low temperatures. Ideally, purely electrically driven valleytronics through VHE and inverse VHE will reduce device footprint, but it remains challenging to improve the efficiency of valley-charge conversion.[109,126,130] For instance, the inverse scaling of the Berry curvature with bandgap indicates a direct increase of VHE in small-gap semiconductors, but the operation temperatures may need to be kept low to suppress current leakage. Therefore, fine-tuning of bandgap in novel materials is imperative to construct VHE devices, in addition to high mobility and long diffusion length. Interestingly, the choice of materials may be expanded to systems with both inversion and time reversal symmetry based on a new proposal of nonlinear

valley hall effect to detect and manipulate the valley degree of freedom protected with inversion and time reversal symmetry.[130] Although the topic is beyond the scope of this review, we want to emphasize the need to design new device structures and improve device processing techniques based on new materials physics discovered in valleytronic materials.

In short, the field of valleytronics remains in its nascent stages, necessitating concerted efforts to both realize novel materials and construct new devices. Such a comprehensive co-design approach is essential to advance the practical application of the valley degree of freedom in information processing and storage.

Acknowledgements

R.X. and H.Z. acknowledges the support from Welch Foundation (C-2128). H.Z. also acknowledges the support from the National Science Foundation (DMR-2327827). J.L. acknowledges the funding support from the National Natural Science Foundation of China (52102219 and 52471197), and Natural Science Foundation of Shanghai (21ZR1404900).

Conflict of Interest

The authors declare no conflict of interest.

Author Contributions

R.X. and Z.Z. contributed equally to this work. J.L. and H.Z. conceived the idea and supervised the project. All authors contributed to writing the paper.

Keywords

2D Materials, heterostructures, relaxation dynamics, spin-orbit coupling, valleytronics

Received: March 18, 2024
Revised: November 3, 2024
Published online:

[1] K. Behnia, *Nat. Nanotechnol.* **2012**, *7*, 488.
[2] J. Xin, Y. Tang, Y. Liu, X. Zhao, H. Pan, T. Zhu, *npj Quant Mater.* **2018**, *3*, 9.
[3] J. R. Schaibley, H. Yu, G. Clark, P. Rivera, J. S. Ross, K. L. Seyler, W. Yao, X. Xu, *Nat. Rev. Mater.* **2016**, *1*, 16055.
[4] L. Feng, X. Chen, J. Qi, *Phys. Rev. B* **2023**, *108*, 115407.
[5] T. Ye, Y. Li, J. Li, H. Shen, J. Ren, C.-Z. Ning, D. Li, *Light: Sci. Appl.* **2022**, *11*, 23.
[6] C. Jin, J. Kim, M. I. B. Utama, E. C. Regan, H. Kleemann, H. Cai, Y. Shen, M. J. Shinner, A. Sengupta, K. Watanabe, T. Taniguchi, S. Tongay, A. Zettl, F. Wang, *Science* **2018**, *360*, 893.
[7] J. Isberg, M. Gabrysch, J. Hammersberg, S. Majdi, K. K. Kovi, D. J. Twitchen, *Nat. Mater.* **2013**, *12*, 760.
[8] D. Culcer, A. L. Saraiva, B. Koiller, X. Hu, S. Das Sarma, *Phys. Rev. Lett.* **2012**, *108*, 126804.
[9] K. Takashina, Y. Ono, A. Fujiwara, Y. Takahashi, Y. Hirayama, *Phys. Rev. Lett.* **2006**, *96*, 236801.
[10] C. H. Yang, A. Rossi, R. Ruskov, N. S. Lai, F. A. Mohiyaddin, S. Lee, C. Tahan, G. Klimeck, A. Morello, A. S. Dzurak, *Nat. Commun.* **2013**, *4*, 2069.
[11] N. C. Bishop, M. Padmanabhan, K. Vakili, Y. P. Shkolnikov, E. P. De Poortere, M. Shayegan, *Phys. Rev. Lett.* **2007**, *98*, 266404.
[12] Z. Zhu, A. Collaudin, B. Fauqué, W. Kang, K. Behnia, *Nat. Phys.* **2012**, *8*, 89.
[13] A. Rycerz, J. Tworzydło, C. W. J. Beenakker, *Nat. Phys.* **2007**, *3*, 172.
[14] D. Xiao, W. Yao, Q. Niu, *Phys. Rev. Lett.* **2007**, *99*, 236809.
[15] D. Xiao, G.-B. Liu, W. Feng, X. Xu, W. Yao, *Phys. Rev. Lett.* **2012**, *108*, 196802.
[16] H. Zeng, J. Dai, W. Yao, D. Xiao, X. Cui, *Nat. Nanotechnol.* **2012**, *7*, 490.
[17] T. Cao, G. Wang, W. Han, H. Ye, C. Zhu, J. Shi, Q. Niu, P. Tan, E. Wang, B. Liu, J. Feng, *Nat. Commun.* **2012**, *3*, 887.
[18] K. F. Mak, K. He, J. Shan, T. F. Heinz, *Nat. Nanotechnol.* **2012**, *7*, 494.
[19] Y. Ye, J. Xiao, H. Wang, Z. Ye, H. Zhu, M. Zhao, Y. Wang, J. Zhao, X. Yin, X. Zhang, *Nat. Nanotechnol.* **2016**, *11*, 598.
[20] S. A. Vitale, D. Nezich, J. O. Varghese, P. Kim, N. Gedik, P. Jarillo-Herrero, D. Xiao, M. Rothschild, *Small* **2018**, *14*, 1801483.
[21] F. Bussolotti, H. Kawai, Z. E. Ooi, V. Chellappan, D. Thian, A. L. C. Pang, K. E. J. Goh, *Nano Futures* **2018**, *2*, 032001.
[22] A. Ciarrocchi, F. Tagarelli, A. Avsar, A. Kis, *Nat. Rev. Mater.* **2022**, *7*, 449.
[23] S. Zhao, X. Li, B. Dong, H. Wang, H. Wang, Y. Zhang, Z. Han, H. Zhang, *Rep. Prog. Phys.* **2021**, *84*, 026401.
[24] Y. Liu, Y. Gao, S. Zhang, J. He, J. Yu, Z. Liu, *Nano Res.* **2019**, *12*, 2695.
[25] D. Lagarde, L. Bouet, X. Marie, C. R. Zhu, B. L. Liu, T. Amand, P. H. Tan, B. Urbaszek, *Phys. Rev. Lett.* **2014**, *112*, 047401.
[26] Q. Wang, S. Ge, X. Li, J. Qiu, Y. Ji, J. Feng, D. Sun, *ACS Nano* **2013**, *7*, 11087.
[27] E. H. Hwang, B. Y.-K. Hu, S. Das Sarma, *Phys. Rev. B.* **2007**, *76*, 115434.
[28] M. Amani, D.-H. Lien, D. Kiriya, J. Xiao, A. Azcatl, J. Noh, S. R. Madhvapathy, R. Addou, S. KC, M. Dubey, K. Cho, R. M. Wallace, S.-C. Lee, J.-H. He, J. W. Ager, X. Zhang, E. Yablonovitch, A. Javey, *Science* **2015**, *350*, 1065.
[29] C. Jin, J. Kim, K. Wu, B. Chen, E. S. Barnard, J. Suh, Z. Shi, S. G. Drapcho, J. Wu, P. J. Schuck, S. Tongay, F. Wang, *Adv. Funct. Mater.* **2017**, *27*, 1601741.
[30] T. Yan, S. Yang, D. Li, X. Cui, *Phys. Rev. B.* **2017**, *95*, 241406.
[31] P. Dey, L. Yang, C. Robert, G. Wang, B. Urbaszek, X. Marie, S. A. Crooker, *Phys. Rev. Lett.* **2017**, *119*, 137401.
[32] R. Garreis, C. Tong, J. Terle, M. J. Ruckriegel, J. D. Gerber, L. M. Gächter, K. Watanabe, T. Taniguchi, T. Ihn, K. Ensslin, W. W. Huang, *Nat. Phys.* **2024**, *20*, 428.
[33] D. B. McWhan, P. Hu, M. A. Chin, V. Narayanamurti, *Phys. Rev. B.* **1982**, *26*, 4774.
[34] S. Li, Y. Chen, *Sci. Rep.* **2017**, *7*, 43956.
[35] M. Z. Maialle, E. A. de Andrada e Silva, L. J. Sham, *Phys. Rev. B.* **1993**, *47*, 15776.
[36] M.-S. Song, H. Wang, Z.-F. Hu, Y.-P. Zhang, T.-Y. Liu, H.-Y. Wang, *Adv. Sci.* **2023**, *10*, 2302554.
[37] W. Tao, Q. Zhou, H. Zhu, *Sci. Adv.* **2020**, *6*, abb7132.
[38] T. Cheiwchanchamnangij, W. R. L. Lambrecht, *Phys. Rev. B.* **2012**, *85*, 205302.
[39] H. Shi, H. Pan, Y.-W. Zhang, B. I. Yakobson, *Phys. Rev. B.* **2013**, *87*, 155304.
[40] T. Yu, M. W. Wu, *Phys. Rev. B.* **2014**, *89*, 205303.
[41] E. C. Regan, D. Wang, E. Y. Paik, Y. Zeng, L. Zhang, J. Zhu, A. H. MacDonald, H. Deng, F. Wang, *Nat. Rev. Mater.* **2022**, *7*, 778.
[42] G. Wang, L. Bouet, D. Lagarde, M. Vidal, A. Balocchi, T. Amand, X. Marie, B. Urbaszek, *Phys. Rev. B.* **2014**, *90*, 075413.
[43] C. Mai, A. Barrette, Y. Yu, Y. G. Semenov, K. W. Kim, L. Cao, K. Gundogdu, *Nano Lett.* **2014**, *14*, 202.
[44] C. Mai, Y. G. Semenov, A. Barrette, Y. Yu, Z. Jin, L. Cao, K. W. Kim, K. Gundogdu, *Phys. Rev. B.* **2014**, *90*, 041414.

[45] G. Plechinger, P. Nagler, C. Schüller, T. Korn, *arXiv* **2014**, 1404.7674.
[46] C. R. Zhu, K. Zhang, M. Glazov, B. Urbaszek, T. Amand, Z. W. Ji, B. L. Liu, X. Marie, *Phys. Rev. B.* **2014**, *90*, 161302.
[47] S. Dal Conte, F. Bottegoni, E. A. A. Pogna, D. De Fazio, S. Ambrogio, I. Bargigia, C. D'Andrea, A. Lombardo, M. Bruna, F. Ciccacci, A. C. Ferrari, G. Cerullo, M. Finazzi, *Phys. Rev. B.* **2015**, *92*, 235425.
[48] K. Hao, G. Moody, F. Wu, C. K. Dass, L. Xu, C.-H. Chen, L. Sun, M.-Y. Li, L.-J. Li, A. H. MacDonald, X. Li, *Nat. Phys.* **2016**, *12*, 677.
[49] F. Mahmood, Z. Alpichshev, Y.-H. Lee, J. Kong, N. Gedik, *Nano Lett.* **2018**, *18*, 223.
[50] Y. Jiang, S. Chen, W. Zheng, B. Zheng, A. Pan, *Light: Sci. Appl.* **2021**, *10*, 72.
[51] J. Kunstmann, F. Mooshammer, P. Nagler, A. Chaves, F. Stein, N. Paradiso, G. Plechinger, C. Strunk, C. Schüller, G. Seifert, D. R. Reichman, T. Korn, *Nat. Phys.* **2018**, *14*, 801.
[52] P. Rivera, J. R. Schaibley, A. M. Jones, J. S. Ross, S. Wu, G. Aivazian, P. Klement, K. Seyler, G. Clark, N. J. Ghimire, J. Yan, D. G. Mandrus, W. Yao, X. Xu, *Nat. Commun.* **2015**, *6*, 6242.
[53] K. F. Mak, J. Shan, *Nat. Nanotechnol.* **2018**, *13*, 974.
[54] P. Rivera, K. L. Seyler, H. Yu, J. R. Schaibley, J. Yan, D. G. Mandrus, W. Yao, X. Xu, *Science* **2016**, *351*, 688.
[55] W.-T. Hsu, Y.-L. Chen, C.-H. Chen, P.-S. Liu, T.-H. Hou, L.-J. Li, W.-H. Chang, *Nat. Commun.* **2015**, *6*, 8963.
[56] K. Shinokita, X. Wang, Y. Miyauchi, K. Watanabe, T. Taniguchi, S. Konabe, K. Matsuda, *Phys. Rev. B.* **2019**, *100*, 161304.
[57] E. J. Sie, A. J. Frenzel, Y.-H. Lee, J. Kong, N. Gedik, *Phys. Rev. B.* **2015**, *92*, 125417.
[58] Y. You, X.-X. Zhang, T. C. Berkelbach, M. S. Hybertsen, D. R. Reichman, T. F. Heinz, *Nat. Phys.* **2015**, *11*, 477.
[59] F. J. Ohkawa, Y. Uemura, *J. Phys. Soc. Jpn.* **1977**, *43*, 907.
[60] L. J. Sham, S. J. Allen, A. Kamgar, D. C. Tsui, *Phys. Rev. Lett.* **1978**, *40*, 472.
[61] O. Gunawan, Y. P. Shkolnikov, K. Vakili, T. Gokmen, E. P. De Poortere, M. Shayegan, *Phys. Rev. Lett.* **2006**, *97*, 186404.
[62] Y. P. Shkolnikov, E. P. De Poortere, E. Tutuc, M. Shayegan, *Phys. Rev. Lett.* **2002**, *89*, 226805.
[63] L. L. Tao, E. Y. Tsymbal, *Phys. Rev. B.* **2019**, *100*, 161110.
[64] C. J. Ciccarino, T. Christensen, R. Sundararaman, P. Narang, *Nano Lett.* **2018**, *18*, 5709.
[65] L. Yang, N. A. Sinitsyn, W. Chen, J. Yuan, J. Zhang, J. Lou, S. A. Crooker, *Nat. Phys.* **2015**, *11*, 830.
[66] J. Kim, C. Jin, B. Chen, H. Cai, T. Zhao, P. Lee, S. Kahn, K. Watanabe, T. Taniguchi, S. Tongay, M. F. Crommie, F. Wang, *Sci. Adv.* **2017**, *3*, 1700518.
[67] H. Ochoa, R. Roldán, *Phys. Rev. B.* **2013**, *87*, 245421.
[68] J. Zhou, M. W. Wu, *Phys. Rev. B.* **2008**, *77*, 075318.
[69] M. I. Dyakonov, V. I. Perel', *Soviet J. Exp. Theor. Phys.* **1971**, *33*, 1053.
[70] L. Wang, M. W. Wu, *Phys. Rev. B.* **2014**, *89*, 115302.
[71] Y. Song, H. Dery, *Phys. Rev. Lett.* **2013**, *111*, 026601.
[72] T. Yan, X. Qiao, P. Tan, X. Zhang, *Sci. Rep.* **2015**, *5*, 15625.
[73] J. Xu, A. Habib, S. Kumar, F. Wu, R. Sundararaman, Y Ping, *Nat. Commun.* **2020**, *11*, 2780.
[74] C. Jin, E. Y. Ma, O. Karni, E. C. Regan, F. Wang, T. F. Heinz, *Nat. Nanotechnol.* **2018**, *13*, 994.
[75] Z. Jin, X. Li, J. T. Mullen, K. W. Kim, *Phys. Rev. B* **2014**, *90*, 045422.
[76] N. F. Hinsche, A. S. Ngankeu, K. Guilloy, S. K. Mahatha, A. Grubišić Čabo, M. Bianchi, M. Dendzik, C. E. Sanders, J. A. Miwa, H. Bana, E. Travaglia, P. Lacovig, L. Bignardi, R. Larciprete, A. Baraldi, S. Lizzit, K. S. Thygesen, P. Hofmann, *Phys. Rev. B.* **2017**, *96*, 121402.
[77] T.-Y. Jeong, S. Bae, S.-Y. Lee, S. Jung, Y.-H. Kim, K.-J. Yee, *Nanoscale* **2020**, *12*, 22487.
[78] X. Li, J. T. Mullen, Z. Jin, K. M. Borysenko, M. Buongiorno Nardelli, K. W. Kim, *Phys. Rev. B.* **2013**, *87*, 115418.
[79] L. Ju, Z. Shi, N. Nair, Y. Lv, C. Jin, J. Velasco, C. Ojeda-Aristizabal, H. A. Bechtel, M. C. Martin, A. Zettl, J. Analytis, F. Wang, *Nature* **2015**, *520*, 650.
[80] R. V. Gorbachev, J. C. W. Song, G. L. Yu, A. V. Kretinin, F. Withers, Y. Cao, A. Mishchenko, I. V. Grigorieva, K. S. Novoselov, L. S. Levitov, A. K. Geim, *Science* **2014**, *346*, 448.
[81] S. Wu, C. Huang, G. Aivazian, J. S. Ross, D. H. Cobden, X. Xu, *ACS Nano* **2013**, *7*, 2768.
[82] B. Yan, Q. Han, Z. Jia, J. Niu, T. Cai, D. Yu, X. Wu, *Phys. Rev. B.* **2016**, *93*, 041407.
[83] V. Lordi, P. Erhart, D. Åberg, *Phys. Rev. B.* **2010**, *81*, 235204.
[84] H. Tian, C. Ren, S. Wang, *Nanotechnology* **2022**, *33*, 212001.
[85] E. Yamaguchi, *J. Appl. Phys.* **1984**, *56*, 1722.
[86] G. Moody, K. Tran, X. Lu, T. Autry, J. M. Fraser, R. P. Mirin, L. Yang, X. Li, K. L. Silverman, *Phys. Rev. Lett.* **2018**, *121*, 057403.
[87] N. Rana, G. Dixit, *Phys. Rev. Appl.* **2023**, *19*, 034056.
[88] R. E. F. Silva, M. Ivanov, Á. Jiménez-Galán, *Opt. Express* **2022**, *30*, 30347.
[89] F. Langer, C. P. Schmid, S. Schlauderer, M. Gmitra, J. Fabian, P. Nagler, C. Schüller, T. Korn, P. G. Hawkins, J. T. Steiner, U. Huttner, S. W. Koch, M. Kira, R. Huber, *Nature* **2018**, *557*, 76.
[90] Z. Ye, D. Sun, T. F. Heinz, *Nat. Phys.* **2017**, *13*, 26.
[91] M. S. Mrudul, Á. Jiménez-Galán, M. Ivanov, G. Dixit, *Optica* **2021**, *8*, 422.
[92] Q. Zhang, H. Sun, J. Tang, X. Dai, Z. Wang, C.-Z. Ning, *Nat. Commun.* **2022**, *13*, 4101.
[93] M. Ezawa, *Phys. Rev. B.* **2013**, *87*, 155415.
[94] Y. Yang, X. Cheng, L. Xiao, S. Jia, J. Chen, L. Zhang, J. Wang, *Phys. Rev. B.* **2024**, *109*, 235403.
[95] H. Zhou, T. Xie, A. Ghazaryan, T. Holder, J. R. Ehrets, E. M. Spanton, T. Taniguchi, K. Watanabe, E. Berg, M. Serbyn, A. F. Young, *Nature* **2021**, *598*, 429.
[96] S. Li, W. Wu, X. Feng, S. Guan, W. Feng, Y. Yao, S. A. Yang, *Phys. Rev. B.* **2020**, *102*, 235435.
[97] J. Liang, Q. Fang, H. Wang, R. Xu, S. Jia, Y. Guan, Q. Ai, G. Gao, H. Guo, K. Shen, X. Wen, T. Terlier, G. P. Wiederrecht, X. Qian, H. Zhu, J. Lou, *Adv. Mater.* **2020**, *32*, 2004111.
[98] S. Li, J. He, L. Grajciar, P. Nachtigall, *J. Mater. Chem. C.* **2021**, *9*, 11132.
[99] Z.-M. Yu, S. Guan, X.-L. Sheng, W. Gao, S. A. Yang, *Phys. Rev. Lett.* **2020**, *124*, 037701.
[100] J. Y. Liu, J. Yu, J. L. Ning, H. M. Yi, L. Miao, L. J. Min, Y. F. Zhao, W. Ning, K. A. Lopez, Y. L. Zhu, T. Pillsbury, Y. B. Zhang, Y. Wang, J. Hu, H. B. Cao, B. C. Chakoumakos, F. Balakirev, F. Weickert, M. Jaime, Y. Lai, K. Yang, J. W. Sun, N. Alem, V. Gopalan, C. Z. Chang, N. Samarth, C. X. Liu, R. D. McDonald, Z. Q. Mao, *Nat. Commun.* **2021**, *12*, 4062.
[101] J. Liang, Q. Ai, X. Wen, X. Tang, T. Zhai, R. Xu, X. Zhang, Q. Fang, C. Nguyen, Y. Liu, H. Zhu, T. Terlier, G. P. Wiederrecht, P. M. Ajayan, X. Qian, J. Lou, *Mater. Today* **2024**, *74*, 77.
[102] K. Takeda, K. Shiraishi, *Phys. Rev. B.* **1994**, *50*, 14916.
[103] C.-C. Liu, W. Feng, Y. Yao, *Phys. Rev. Lett.* **2011**, *107*, 076802.
[104] P. Vogt, P. De Padova, C. Quaresima, J. Avila, E. Frantzeskakis, M. C. Asensio, A. Resta, B. Ealet, G. Le Lay, *Phys. Rev. Lett.* **2012**, *108*, 155501.
[105] M. Ezawa, *New J. Phys.* **2012**, *14*, 033003.
[106] M. Ezawa, *Phys. Rev. Lett.* **2012**, *109*, 055502.
[107] J. Yin, C. Tan, D. Barcons-Ruiz, I. Torre, K. Watanabe, T. Taniguchi, J. C. W. Song, J. Hone, F. H. L. Koppens, *Science* **2022**, *375*, 1398.
[108] L. Ju, L. Wang, X. Li, S. Moon, M. Ozerov, Z. Lu, T. Taniguchi, K. Watanabe, E. Mueller, F. Zhang, D. Smirnov, F. Rana, P. L. McEuen, *Nat. Commun.* **2020**, *11*, 2941.
[109] J. Lee, W. Heo, M. Cha, K. Watanabe, T. Taniguchi, J. Kim, S. Cha, D. Kim, M.-H. Jo, H. Choi, *Nat. Commun.* **2021**, *12*, 1635.

[110] T. Y. T. Hung, K. Y. Camsari, S. Zhang, P. Upadhyaya, Z. Chen, *Sci. Adv.* **2019**, *5*, aau6478.
[111] J. M. Park, Y. Cao, K. Watanabe, T. Taniguchi, P. Jarillo-Herrero, *Nature* **2021**, *590*, 249.
[112] G. Chen, *Quantum Front.* **2022**, *1*, 8.
[113] F. Zhang, B. Sahu, H. Min, A. H. MacDonald, *Phys. Rev. B.* **2010**, *82*, 035409.
[114] Y.-L. Hong, Z. Liu, L. Wang, T. Zhou, W. Ma, C. Xu, S. Feng, L. Chen, M.-L. Chen, D.-M. Sun, X.-Q. Chen, H.-M. Cheng, W. Ren, *Science* **2020**, *369*, 670.
[115] J. Zhou, J. Lin, H. Sims, C. Jiang, C. Cong, J. A. Brehm, Z. Zhang, L. Niu, Y. Chen, Y. Zhou, Y. Wang, F. Liu, C. Zhu, T. Yu, K. Suenaga, R. Mishra, S. T. Pantelides, Z.-G. Zhu, W. Gao, Z. Liu, W. Zhou, *Adv. Mater.* **2020**, *32*, 1906536.
[116] Q. Zhang, S. A. Yang, W. Mi, Y. Cheng, U. Schwingenschlögl, *Adv. Mater.* **2016**, *28*, 959.
[117] X. Feng, Z. He, R. Peng, Y. Dai, B. Huang, Y. Ma, *Phys. Rev. Mater.* **2022**, *6*, 044001.
[118] J. Guo, Z. Lu, K. Wang, X. Zhao, G. Hu, X. Yuan, J. Ren, *J. Phys.: Condens. Matter* **2021**, *34*, 075701.
[119] Y. Shimazaki, M. Yamamoto, I. V. Borzenets, K. Watanabe, T. Taniguchi, S. Tarucha, *Nat. Phys.* **2015**, *11*, 1032.
[120] Y. J. Zhang, T. Oka, R. Suzuki, J. T. Ye, Y. Iwasa, *Science* **2014**, *344*, 725.
[121] Z. Tian, C. Guo, M. Zhao, R. Li, J. Xue, *ACS Nano* **2017**, *11*, 2219.
[122] Q. Zhang, U. Schwingenschlögl, *Phys. Rev. B* **2018**, *97*, 155415.
[123] K. Lee, W. S. Yun, J. D. Lee, *Phys. Rev. B.* **2015**, *91*, 125420.
[124] B. Sanchez-Lengeling, A. Aspuru-Guzik, *Science* **2018**, *361*, 360.
[125] H. Zhu, J. Yi, M.-Y. Li, J. Xiao, L. Zhang, C.-W. Yang, R. A. Kaindl, L.-J. Li, Y. Wang, X. Zhang, *Science* **2018**, *359*, 579.
[126] K. F. Mak, K. L. McGill, J. Park, P. L. McEuen, *Science* **2014**, *344*, 1489.
[127] Y. S. Ang, S. A. Yang, C. Zhang, Z. Ma, L. K. Ang, *Phys. Rev. B.* **2017**, *96*, 245410.
[128] L. Li, L. Shao, X. Liu, A. Gao, H. Wang, B. Zheng, G. Hou, K. Shehzad, L. Yu, F. Miao, Y. Shi, Y. Xu, X. Wang, *Nat. Nanotechnol.* **2020**, *15*, 743.
[129] S. Lai, Z. Zhang, N. Wang, A. Rasmita, Y. Deng, Z. Liu, W. Gao, *Nano Lett.* **2023**, *23*, 192.
[130] K. Das, K. Ghorai, D. Culcer, A. Agarwal, *Phys. Rev. Lett.* **2024**, *132*, 096302.

Rui Xu received his Ph.D. from the Department of Material Science & NanoEngineering at Rice University. His research interest focuses on optical spectroscopy of nanomaterials.

Zhiguo Zhang works in the Department of Materials Science at Fudan University as a postdoctoral fellow from 2023. He obtained his Ph.D. in nanotechnology & applied physics from University of Twente, Netherlands, in 2022. His research interests include the synthesis and detailed characterization of nanostructure, 2D materials and alloys, as well as exploration of fundamental physics of surface and interfaces.

Jia Liang is an associate professor in the Department of Materials Science at Fudan University, China. He earned his B.E. in physics from Southeast University and his Ph.D. degree in Physical Electronics from Peking University. Prior to joining Fudan University, he did his postdoctoral research at the Smalley-Curl Institute at Rice University. His research interests include the fabrication of low-dimensional materials and their applications in valleytronics.

Hanyu Zhu is an assistant professor in materials science and nanoengineering at Rice University starting in 2018. He received Ph.D. in the Applied Science and Technology program at the University of California, Berkeley in 2016. He studies quantum materials and their emergent properties, such as the coupling between the spin-orbit states of electrons and lattices, using nonlinear optics and ultrafast spectroscopy for photonic, optoelectronic, and spintronic devices in both classical and quantum regime.